THESIS FOR THE DEGREE OF DOCTOR OF PHILOSOPHY

Development of new nanomaterials syntheses for mesostructured TiO_2 and SiO_2

Erik Nilsson

Department of Chemical and Biological Engineering
CHALMERS UNIVERSITY OF TECHNOLOGY
Göteborg, Sweden
2011

Development of new nanomaterials syntheses for mesostructured TiO_2 and SiO_2

Development of new nanomaterials syntheses for mesostructured TiO_2 and SiO_2

ERIK NILSSON

ISBN 978-91-7385-553-2

Doktorsavhandlingar vid Chalmers tekniska högskola
Ny serie nr 3234

ISSN 0346-718X

Department of Chemical and Bilogical Engineering
Chalmers University of Technology
SE-412 96 Göteborg
Sweden
Telephone + 46 (0)31-772 1000

Cover: *Scanning Electron Microscopy picture of a titania film and Transmission Electron Microscopy magnifications showing the hexagonal mesoordered pores and the crystal lattice fringes of the crystallites within the pore wall.*

Printed by:
Reproservice
Göteborg, Sweden 2011

Erik Nilsson
Department of Chemical and Biological Engineering
Chalmers University of Technology

Abstract

Mesostructured materials is a class of materials within the concept nanomaterials and characterized by structural features on the length scale 2-50 nm. This group of materials is interesting for several applications such as, membrane and separation technology, heterogeneous catalysis, controlled release, adsorption of pollutants, solar energy conversion, electrode materials etc. These materials can be prepared with a wide range of chemical compositions. The thesis focuses on syntheses of mesostructured silica and titania.

The interests for mesostructured materials is growing and the need for low cost large scale production methods is becoming interestingly important. An alkaline silicate solution, also called waterglass, is a cheap silica source that has been studied for this purpose. Mesostructured materials are formed using a structure directing supramolecular assembly as template. These are either based on surfactants or block-copolymers and for a large scale application, nonionic amphiphiles are desired. Synthesis methods for mesostructured silica require tuning the conditions for inducing the gelation of the silica monomers within the amphiphilic liquid crystal template. The gelation behavior of water glass has therefore been studied by adjusting pH or solvent evaporation and found to be fundamentally different for this. Following this a study of the liquid crystal formation of waterglass and nonionic surfactant mixtures has been examined and the first direct synthesis of mesostructured silica from alkaline water glass and non-ionic block-copolymers developed.

Titanium dioxide is a photoactive semiconductor in its crystalline state. Mesoordered crystalline titania is desired in photovoltaic and photocatalytic applications. However, titania normally crystalises through solid state reactions at several hundred degrees centigrade, whereas liquid crystals that are used for templating mesoorder exist at much lower temperatures as aqueous mixtures. A low temperature microemulsion synthesis of nanoparticulate crystalline titania was developed and further modified into a new direct synthesis methodology for the preparation of mesoporous titania with hexagonal mesostructure and with walls of tunable crystallinity and crystallite size.

List of Publications

I. **Concentration- and pH-dependence of highly alkaline sodium silicate solutions**
Jonas Nordström, Erik Nilsson, Patrik Jarvol, Moheb Nayeri, Anders E. C. Palmqvist, Johan Bergenholtz, Aleksandar Matic
Journal of Colloid and Interface Science, **2011**, 356, 37-45

II. **Synthesis of ordered mesostructured SiO_2 using alkaline waterglass and nonionic amphiphilics**
Erik Nilsson, Hirotoshi Furusho, Andreas Sundblom, Osamu Terasaki, Anders E. C. Palmqvist
Manuscript

III. **Synthesis of nano-particulate anatase and rutile crystallites at low temperatures in the Pluronic F127 microemulsion system**
Erik Nilsson, Hirotoshi Furusho, Osamu Terasaki, Anders E. C. Palmqvist
Journal of Materials Research, **2011,** 26, 1-8

IV. **Low temperature synthesis and HRTEM analysis of ordered mesoporous anatase with tunable crystallite size and pore shape**
Erik Nilsson, Yasuhiro Sakamoto, Anders E. C Palmqvist
Chemistry of Materials, **2011,** DOI: 10.1021/cm103600q

Contribution Report

I Responsible for all preparatory work, partly responsible for ^{29}Si-NMR measurements, and interpreting data and partly responsible for writing the manuscript.

II Responsible for writing the manuscript and for all experimental and analytical work except for collecting the TEM-images in Figure 7.

III Responsible for writing the manuscript and for all synthesis work and PXRD-measurements.

IV Responsible for writing the manuscript and for all synthesis work and partly responsible for the TEM-analysis.

Table of Contents

1. INTRODUCTION

Nanomaterials are becoming more and more common in our daily environment. Their application areas include construction materials, pharmaceuticals, electronics, textiles, paint, energy conversion devices, catalysis, adsorption, and more. Nano is the prefix for 10^{-9}, thus nanostructured materials are materials with characteristic dimensions at the length scale of billionth of a meter. Nano is a widely used term and the need for specified definitions is therefore required. IUPAC have defined nanoporous, which is a topic of this thesis, materials as micro-, meso- or macroporous depending on the size of the pore diameter, where micro < 2nm; 2nm < meso <50 nm and macro > 50 nm.[1]

1.1. BACKGROUND

In the beginning of the 1990´s a new family of nanostructured molecular sieves was reported independently by a Japanese research group[2,3] and the Mobil oil corporation.[4,5] The material, primarily based on SiO_2, had a porous structure within the meso-range that was not randomly oriented but arranged in well ordered hexagonal or cubic mesostructures. These new types of inorganic materials quickly draw a lot of attention which resulted in a rapid increase in number of published papers per year[6], among which several reviews have covered the topic.[6-13] Among the more important progress made during the first years were the use of nonionic block copolymers as structure directing agent, the capability to control the pore size and the syntheses of other types of metal-oxides than SiO_2.[14-21] Additional breakthroughs in the area include the pioneering studies for preparation of ordered metal, carbon and polymers[14,22-25] as well as the development of the evaporation-induced self-assembly process for thin films.[26] The properties of the ordered mesoporous materials make them interesting for a wide area of applications such as catalysis, membrane and separation technology, controlled release, adsorption of pollutants, solar energy conversion, electronic devices like displays and data storage, wine clarification etc.[9,27-37]

1.2. AIM

This thesis deals with synthesis and characterization of nanostructured SiO_2 and TiO_2 with the aim to develop more refined syntheses for these systems with a large potential to be utilized in production of these type of materials. The thesis covers two different materials systems, both with the same long-term objective. That is, to develop new efficient synthesis routes for formation of nanoparticulate and mesoordered materials and to increase the physic-chemical insight to the systems to enable development of these syntheses.

2. SYNTHESIS OF NANOSTRUCTURED MATERIALS

The general term nanomaterial includes both discrete particles and materials that have a structural feature characterized within the nanometer size range. This work includes studies of both nanoparticles and nanoporous material made using wet-chemical methods based on surface-active compounds as structure directing components.

2.1. SURFACTANTS AND THEIR SELF-ASSEMBLY

A surface-active compound is an amphiphilic molecule, i.e. it consists of one hydrophilic and one hydrophobic part. The hydrophobic part, also called tail, is usually a hydrocarbon chain. The hydrophilic part, or head group, can be divided into three main categories; anionic, cationic and nonionic depending on its chemical structure. The nature of surfactants makes them strive to go to interfaces, directing head and tail towards the most hydrophilic and hydrophobic surface respectively.

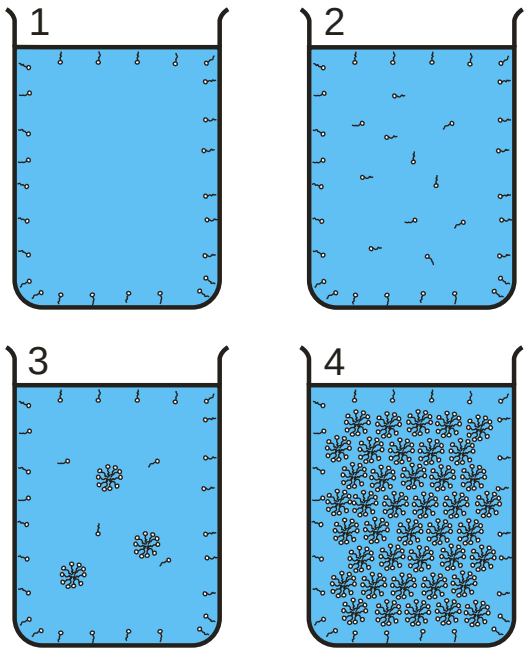

Figure 1. Illustration of the dependence of surfactant self-assembly on surfactant concentration in water. When the concentration increases (1→4) the surfactants first aggregates to micelles and then to liquid crystals.

For example, consider surfactants that are mixed in a glass container of water (Figure 1). The hydrophobic tail will try to avoid the water phase whereas the hydrophilic head group likes the surrounding waterphase. Therefore you will find the surfactants at the air/water- and glass/water-interfaces (1). When the interfaces are saturated the excessive surfactants will exist as free molecules in the solution (2). As the concentration of surfactants in solution increases it

finally reaches a point where no more surfactant can be dissolved and they start to interact. The interaction leads to self-assembly of the surfactants and formation of aggregates. These aggregates are called micelles (3). Micelle formation is a way for the surfactant to remove hydrophobic groups from contact with water and thereby reducing the free energy of the system. When the volume fraction of the micelles is so high that random solutions of micelles cannot exist the micelles start to form supra-molecular structures with long range order called liquid-crystalline phases (4). Depending on concentration various types of liquid crystals such as cubic, hexagonal and lamellar can be formed.

2.2. MICROEMULSION SYNTHESIS OF NANOPARTICLES

By using surfactants it is possible to make a stable dispersion of two liquids that normally are immiscible such as water and oil. Generally, if the main component is water it will be the continuous phase and the oil component will be stabilized, by the surfactants, as small droplets within the micelles. This is called oil in water (o/w) microemulsion. If the oil component is the continuous phase and water is dispersed as droplets it is called an inverse microemulsion (w/o). The small droplets in a microemulsion can be utilized as small reactors in a synthesis using either organic or inorganic reagents. This is done by first mixing two water soluble reactants in two different w/o microemulsions that have the same composition apart from the reactants and then mixing them together. Because of the dynamic equilibrium of the microemulsions, there is as continuous fusion and diffusion of the microemulsion droplets which results in the two reactants being mixed and the reaction taking place within the droplets as illustrated in Figure 2.

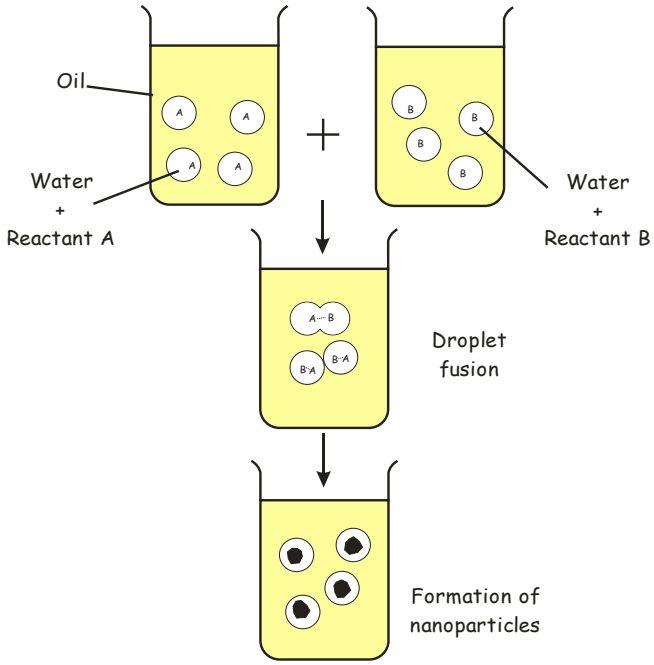

Figure 2. Microemulsion synthesis of nanoparticles where the reactants are both soluble in water.

For the reaction described in Figure 2 both reactants and product are soluble in the aqueous droplets. However, if the reactants have different solubility the reaction will take place at the surface between the microemulsion droplets and the continuous domain (Figure 3).

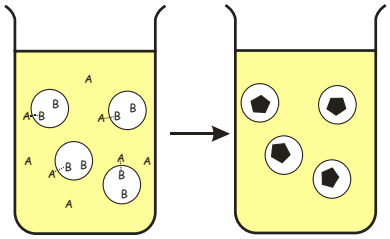

Figure 3. Microemulsion synthesis of nanoparticles where the reactants have different solubility.

2.3. SYNTHESIS OF MESOORDERED MATERIALS

Mesoordered inorganic materials are most often formed in situ with the interaction with inorganic condensating monomers and a surface active compound in a wet-chemical medium.[7,15,23,38] Mesoordered materials can be formed from both micellar and liquid crystalline mixtures.[5,24-26,39-41] In both cases the surfactants are generally subsequently removed by calcination or via washing mixtures and the remaining solid is an ordered mesoporous inorganic material.

2.3.1. FROM MICELLAR SOLUTION

In a micellar solution the reacting inorganic precursors associate with the surfactant during polymerization and precipitate in an ordered arrangement (Figure 4). For these syntheses, where the mesostructured material is formed as a precipitate, the interaction between the inorganic monomers and the surfactants in the solution is critical to achieve the structure-directing effect of the surfactant.

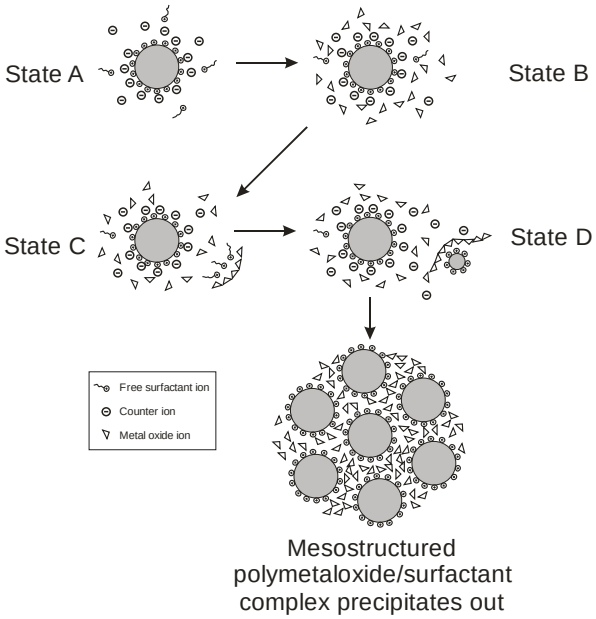

Figure 4. Mesostructured inorganic material formed in a micellar solution. Redrawn from Zana et al.[42]

2.3.2. FROM LIQUID CRYSTAL TEMPLATING

A conceptually more straight forward method is to use liquid crystals as direct templates and let the inorganic monomers polymerize in the water domains of the liquid crystal (Figure 5). In this case the structure directing effect is based only on the cavities formed within the liquid crystal. Interaction between the inorganic precursor and the surfactant is therefore not required and may even negatively affect the phase diagram of the surfactant. In practice this route is more complicated to realize experimentally.

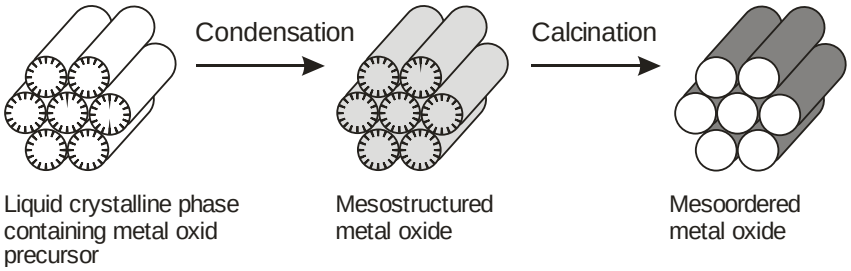

Figure 5. Mesostructured inorganic material formed in a liquid crystalline phase. Redrawn from Berggren et al.[6]

3. CHEMISTRY OF SOLUBLE SILICATES

Silica, expressed as SiO_2, is a general name for silicon dioxide in all its amorphous, crystalline, hydrated or hydroxylated forms.[43] Next to water silica is the most common compound on earth. It exists almost everywhere, in earth and rocks as well as in animals and plants. Solid silica can be dissolved to alkali silica solutions by heating the silica with excess of alkali.

3.1. WATERGLASS

Commercial solutions of alkali silicate solutions are called waterglass. They are characterized by their silica concentration expressed as wt%, type of alkali and its molar- or weight-ratio SiO_2:M_2O ($M=K^+$ or Na^+). Waterglass is an inexpensive source of silica used for applications such as detergents, cements, adhesives and coatings.[43-46] Recently waterglass was used to seal a crack in the reactor shell of one of the nuclear power plants in Fukishima to prevent leakage of radioactive radiation.[47] The use of inorganic silica sources for synthesis of mesoporous materials has become a topic of increased interest to reduce cost compared to the use of alkoxide-based silica sources.[6,39,48,49]

3.1.1. GELATION OF WATERGLASS

A straight-forward method to prepare mesoporous silica would be to mix surfactants and waterglass appropriately concentrated or otherwise adjusted so that a silica gel may form around the surfactant aggregates. However, this is not a trivial exercise, and among the difficulties is to induce gelation and condensation of the silica species to enable the formation of a continuous silica network at a suitable rate.

Gelation through pH-adjustment

The chemistry of soluble silicates and its colloidal stability are somewhat complicated issues. As can be seen from Figure 6, the colloidal stability of soluble silicates is strongly pH-dependent. Interestingly, maximum in colloidal stability exists at the isolelectric point of silica, which is at pH ~2. Below this point the condensation rate is proportional to $[H^+]$ and increases with decreasing pH. In contrast to this the condensation rate is proportional to $[OH^-]$ above the isoelectric point and a minimum in colloidal stability is reached at pH 5-6. When pH is increased above this minimum increased surface charging prevents the colloids to come in contact which leads to increased colloidal stability. Around pH 10.5 silica dissolves and species existing at these conditions are mostly ions such as SiO_3^{2-} and $Si_2O_5^{2-}$ but larger particles have been reported at these conditions for solutions with high silica content.[43,50,51]

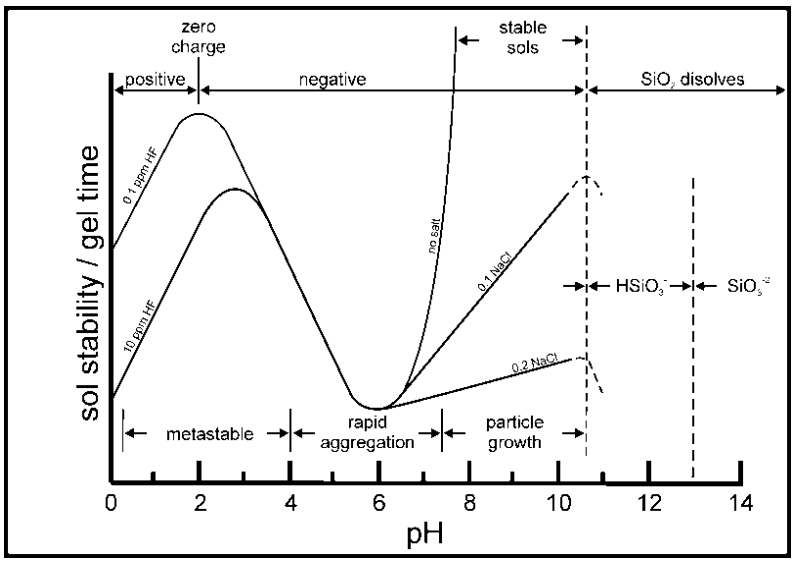

Figure 6. Effects of pH in the colloidal silica-water system redrawn from Iler[43]

Gelation through salt-addition

The presence of salt will lead to screening of surface charges and destabilization of the colloidal solution at pH 7-10 which makes the silica particles come in contact and form a continuous network/gel. If salt is absent the condensation will rather lead to particle growth and maintained colloidal stability. The behavior is described in Figure 7. Because of this, waterglass solutions with low silica:alkali ratio to a higher degree consist of low molecular weight species whereas a high ratio gives stable suspensions of colloidal silica particles.[52,53]

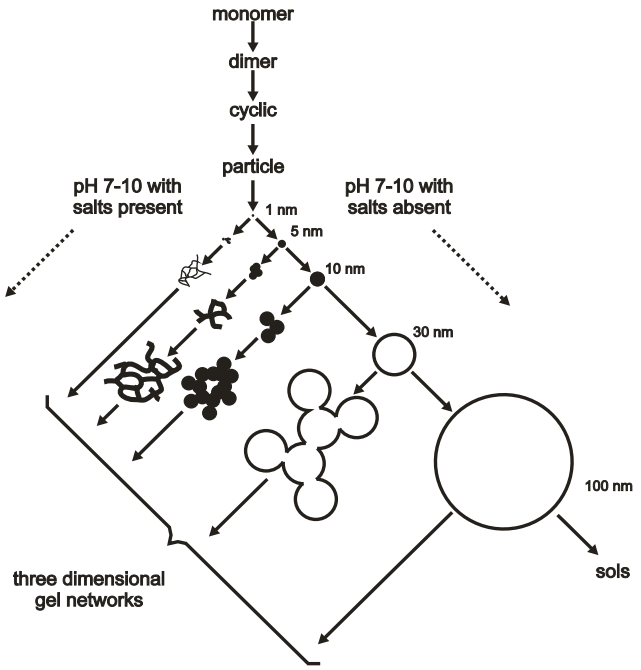

Figure 7. Condensation and gelation behavior of silica redrawn from Iler[43]

Gelation through increased silica concentration

The solubility of silica is not only dependent on pH but also on the silica:alkali ratio and of course the silica concentration. The maximum concentration of commercial sodium silicate solutions is typically around 25 wt%. At these concentrations the solution is still of low viscosity. However, if the concentration is increased to levels above 30 wt% the liquid becomes stiff and shows a gel-like behavior. A few detailed studies on water glass solutions at high concentrations, focusing on the silica:alkali ratio dependence, have been made in the 70´s and 80´s.[51,54]

4. TITANIUM DIOXIDE

The most common daily contact with titanium dioxide is probably as white pigment in paint, plastics, food etc. or as active component in sun screen products. The reason for this is that titania possess a very high refractive index. However, titanium dioxide is also a photoactive semiconductor, and can absorb photons in the UV range wavelength of the solar spectrum. When the material absorbs photons, electron-hole pairs are created by excitation of an electron from the valence band (lower energy state) to the conduction band (higher energy state) and these excited electrons and holes are reactive in photocatalysis and in photovoltaics.

4.1. POLYMORPHS OF TIO_2

The three most common polymorphs (crystal structures) of TiO_2 are brookite, anatase and rutile. Rutile is the most common natural occurring mineral of these three polymorphs. The reason for this is that rutile is thermodynamically stable whereas brookite and anatase are metastable, i. e. brookite and anatase are irreversible converted to rutile upon heating.[55,56] The three polymorphs have different detailed electronic and optical properties.

4.2. PHOTOCATALYTIC PROPERTIES OF TIO_2

4.2.1. WATER SPLITTING

In 1972 the photoelectric properties of TiO_2 was utilized by Honda et al. to achieve photocatalytic water splitting.[57] Upon solar light irradiation of a TiO_2 electrode connected with a platinum electrode in an electrochemical cell they measured current flow via an external circuit. The reactions take place according to the following scheme:

$$TiO_2 + h\nu \rightarrow 2e^- + 2h^+ \qquad (1)$$

$$2h^+ + H_2O \rightarrow \frac{1}{2}O_2 + 2H^+ \qquad (2)$$

$$2H^+ + 2e^- \rightarrow H_2 \qquad (3)$$

Figure 8 illustrates the reduction of water to hydrogen by the free electron in the conduction band and the oxidation of water to oxygen in the valence band.

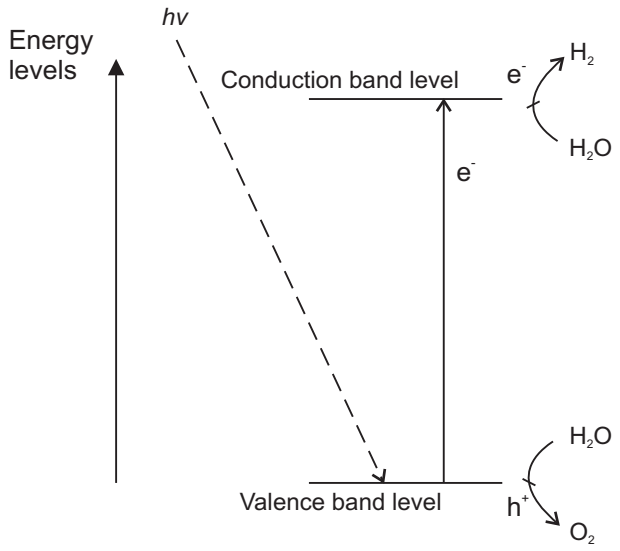

Figure 8. Mechanism of photocatalytic water splitting

4.2.2. DECOMPOSITION OF ORGANIC COMPOUNDS

The photoactive properties of TiO_2 has also been utilized for other applications, such as photocatalytic decomposition of organic compounds in air and waste water[58-64] and bacteria inactivation.[63,65-67] For the use in photocatalytic decomposition a mixture of anatase and rutile is generally considered to be the most effective because of slow electron-hole pair recombination which increase the probability of photocatalytic reaction.[58,68] Anatase is often considered to be more photocatalytically active than rutile.[58,69] However, there are studies that show that rutile nanoparticles synthesized at lower temperatures show similar activity for oxidation but have other reactive paths compared to anatase.[70-72]

4.3. DYESENSITIZED SOLAR CELLS

Another application for TiO_2 is the dye sensitized solar cell(DSSC) developed by Michael Grätzel.[73] The Grätzel cell is a low-cost high efficiency solar cell, based on thin dye impregnated porous films of TiO_2, which has attracted a lot of attention since it was first discovered 1991.[74] The dye has a wider absorption range in the visible region than TiO_2 but the lifespan of the excited electron in the dye is short compared to TiO_2 why a combination of the two components is beneficial. A schematic description of the DSSC is illustrated in Figure 9. The device consists of a mesoporous TiO_2 layer deposited on a glass substrate coated with a conducting transparent film of fluorine-doped tin oxide (FTO). The porous layer is impregnated with a charge transfer dye. The dye absorb the photons and injects the photoexcitated electrons into the conduction band of the TiO_2. The dye is reduced to its ground state by an electrolyte, which most often consists of an

organic solvent containing the $I_3^-/3I^-$ redox pair. The cycle is completed at the platinum cathode where the iodide is reduced to triodide via an external connection through uptake of the free electrons created at the FTO film.

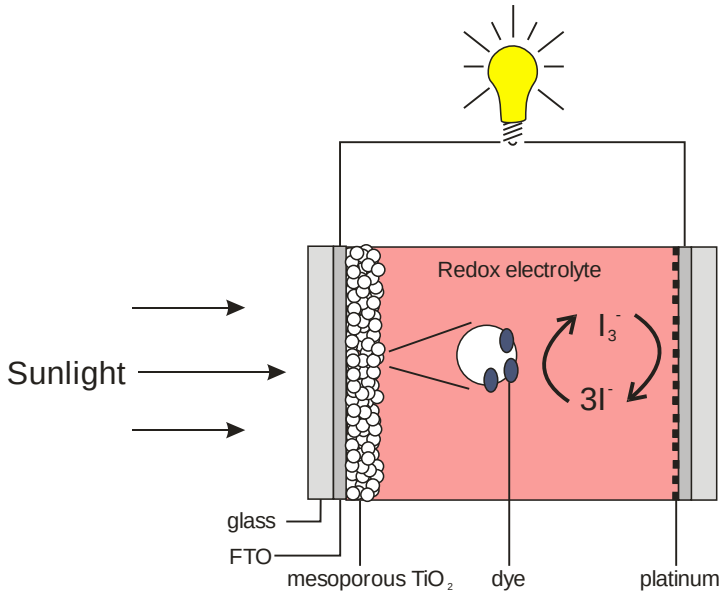

Figure 9. Schematic overview of a dye sensitized solar cell redrawn from Hagfeldt et al.[74]

TiO_2 is only active as long as the photoexcited electron is in the conduction band. It is therefore important, for all photovoltaic applications, to inhibit the electron hole recombination for as long as possible and to increase the probability for reaction to occur. The recombination can be circumvented by increasing the probability for the reaction to occur which is preferably made through an increased concentration of active surface sites, increased connectivity between particles, and between particles and electrode/reactant. This is why ordered mesoporous titania is of interest.[33,75]

5. ANALYTICAL METHODS

Several techniques have been utilized for the characterization and evaluation of materials prepared in this work among which some of these techniques have been performed in cooperation with other researchers. In this chapter basic theory for the methods used by the author is described.

5.1. ^{29}SI-NMR

Nuclear Magnetic Resonance (NMR) spectroscopy has been a very important technique to study the structure and dynamics of molecules since it was first invented about 60 years ago. It is based on the fact that all subatomic particles (electrons, protons and neutrons) of an atom possess a spin. For most isotops, those spins are paired against each other so that the net spin of the nucleus (m) is zero. However, if the number of neutrons and protons is odd the nucleus will possess an overall spin, I, which has the property of being affected by external magnetic fields. Common examples of isotopes that have a spin$\neq$0 are ^{1}H and ^{13}C. According to quantum mechanics the number of possible spin states of an isotope is $2I+1$, e.g. if the spin is ½ it will possess 2 possible orientations. The two spins have equal energy and in an applied external magnetic field the energy level of those spins will split. According to the Boltzmann distribution there will always be slightly more nucleus in the lower energy level. It is possible to excite those spins in the lower energy level to the higher position by exposing this state to a specific radio frequency pulse. One can then detect the relaxation processes of these excited spins as a Free Induction Decay (FID) signal. Via Fourier transformation the FID is transformed from the time domain to the frequency domain in which the NMR spectra are presented.

A nucleus in a magnetic field will precess around the magnetic field. The frequency of this precession is called the *Larmour frequency*, which is specific for each isotope. The nucleus is also affected by a local magnetic field, which is caused by differences in the electronic surrounding experienced by a nucleus in a molecule. The different variations in electronic surroundings give rise to different chemical shifts in the NMR-spectrum, i.e. different frequencies. The local magnetic field experienced by a nucleus may therefore be affected by the physical state (solid or liquid), the viscosity of the solution, the temperature, etc., i.e. the experienced magnetic field is dependent on the motion of the molecule on the microscopic scale. This motion is called the spin-lattice relaxation. Further, spins of different positions but with the same Larmour frequencies can interact in what is called spin-spin relaxation. For more detailed theory regarding

NMR-spectroscopy the book "Nuclear Magnetic Resonance – concepts and methods", by Daniel Canet, is recommended.[76]

For the purpose of studying silicon species, NMR-experiments can only be measured on the isotope ^{29}Si (natural abundance of less than 5%[77]), since the number of protons and neutrons are both even for ^{28}Si. In order to obtain detailed information about the molecular speciation of a sample, several reports have utilized ^{29}Si enriched samples,[77-80] although in the study in this thesis non-enriched samples have been studied.

In ^{29}Si NMR, the tetrahedral coordinated silicon sites are typically designated Q and the number of Si-O-Si bridges to that silicon atom described by a superscript from 0 to 4. For instance Q^0 denotes $[Si(OH)_4]$ and Q^1 $[Si(OH)_3OSi\text{-}]$, etc. The different coordination types of the species give rise to different chemical shifts. A typical spectrum of a sodium silicate solution shows five broad peaks around -70, -79, -88, -97, -107 ppm in chemical shifts corresponding to Q^0, Q^1, Q^2, Q^3 and Q^4, respectively.[50] The shifts are set in comparison to a reference, typically of tetramethylsilane.[81,82] Figure 10 shows a typical spectrum of one of the sodium silicate samples in our study.

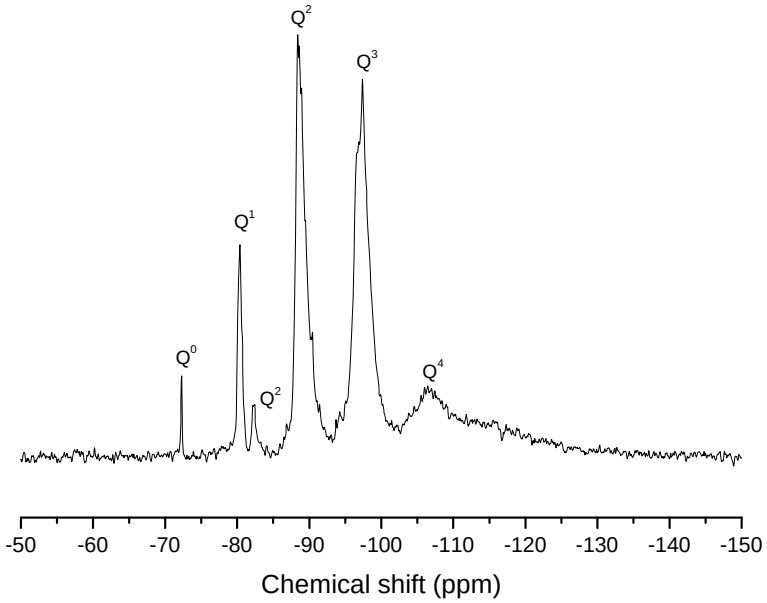

Figure 10. Typical ^{29}Si-NMR spectrum of a sodium silicate solution.

5.2. POWDER X-RAY DIFFRACTION AND SMALL ANGLE X-RAY SCATTERING

In X-ray diffraction a monochromatic X-ray beam is used to probe the structure of a crystal. When the X-ray beam is focused on the sample it is scattered into several beams. The X-ray beams are illustrated as lines in the picture (Figure 11). Beam 2 travels a distance A-B-C longer

than beam 1. If the length of this path is an integer of the wavelength (λ), of the X-ray, the beams will combine interfere constructively and give rise to Bragg peaks. The distance A-B-C depends on the spacing between the crystal planes, d_{hkl}, and the scattering angle, θ, and is expressed in the Bragg-equation:

$$n\lambda = 2d_{hkl}\sin\theta \quad \text{(Bragg's law)}$$

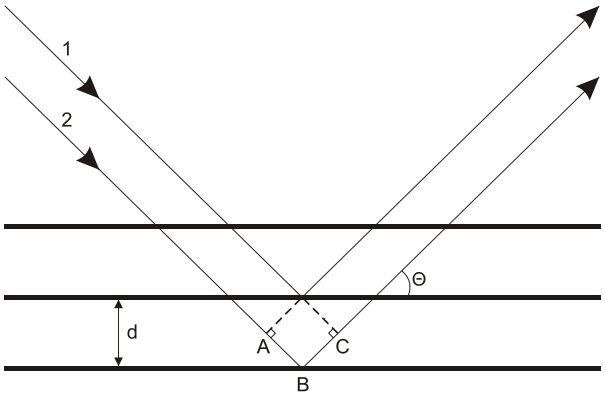

Figure 11. Illustration of Bragg´s law

From the X-ray diffractogram it is also possible to get detailed information about the crystallite size of the sample. When a monochromatic X-ray falls on a crystalline powder sample consisting of small crystallites, the Bragg peaks are broadened when. The mean crystallite size can be calculated according to the Scherrer equation, which relates the crystallite size to the peak-broadening at half maximum intensity.[83,84]

$$D = \frac{K\lambda}{\beta\cos\theta} \quad \text{(The Scherrer equation)}$$

Where D is the mean crystallite diameter, *K* is the Scherrer constant, λ is the wavelength of the X-ray beam, θ the Bragg angle and β the peak width (in 2θ) at half intensity maximum.

Materials with long range order, such as meso-ordered materials or liquid crystals, scatter the incident beam at small angle. Such analysis is referred to as Small Angle X-ray Scattering (SAXS). Just as for normal X-ray scattering the X-rays are scattered by the contrast in electron density of the material, but because the angle is small it is no longer the atomic form factor that is probed but instead the difference in average electron density between nanoscopic objects in the material such as micellar aggregates.

5.3. TRANSMISSION ELECTRON MICROSCOPY

Transmission Electron Microscopy (TEM) is analogous to light microscopy. It consists of an illumination source, a first condenser lens that concentrates the radiation on to the specimen and a series of magnifying lenses. The main difference is that it is electrons instead of photons that generates the image, why the glass-lenses are replaced by electromagnetic fields. The resolution of a microscope is limited by the wavelength of the radiation used. Since electrons have much shorter wavelength than photons the resolution of an electron microscope is also higher and specimen can be studied at magnifications as high as 10^6. After passing through the electromagnetic lenses and the sample the accelerated electrons hit a fluorescent screen on which the image of the specimen appears. If the specimen contains parts of high scattering power, e.g. crystal planes, the electrons will be scattered in angels relative to the incident beam giving rise to a diffraction pattern unique for the specific crystal structure. Just as for the case with X-ray diffraction the beam is scattered by crystal planes represented by electron clouds in the specimen and the diffraction pattern is thus analogous to the corresponding X-ray diffraction pattern. Provided that the microscope is in diffraction mode, illuminating an area of a single crystal will generate a diffraction pattern that will appear bright spots, but if the illuminated area is polycrystalline it will appear as a ring pattern, as illustrated in Figure 12. The Bragg-angle (θ) is calculated by simple geometric analysis from the camera length (L) and the center to ring-distance(X). The crystal plane distance may thus be calculated from Braggs law if the wavelength of the electron beam is known.

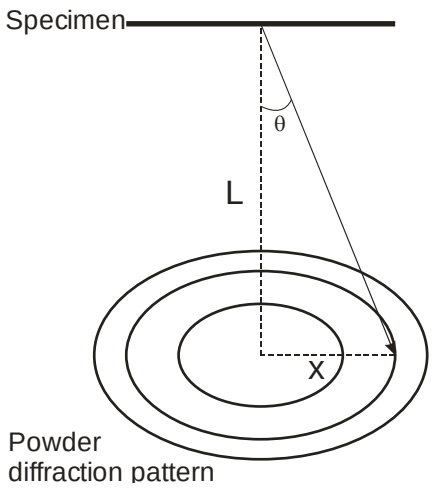

Figure 12. Schematic illustration of generation of a powder diffraction pattern in transmission electron microscopy.

The scattered electrons are normally constrained by the objective aperture and crystalline areas will therefore appear as dark areas on the image. This is called a bright field image. However, if the objective aperture is centered on a diffracted beam, the dark crystalline areas will be bright

and the bright areas will be dark. This is called a dark field image and is illustrated in (Figure 13). Figure 27 on page 36 is a typical example of a bright field micrograph and its corresponding dark field image.

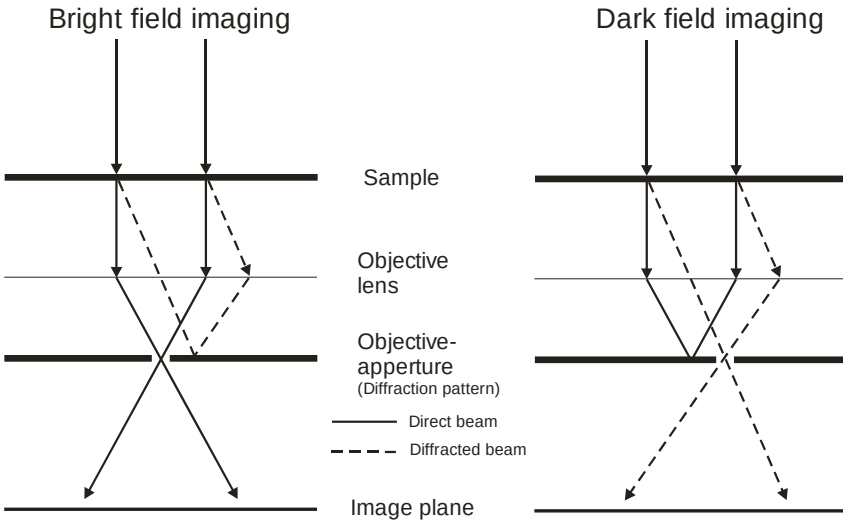

Figure 13. Illustration of creation of bright- and dark-field images in transmission electron microscopy.

5.4. GAS ADSORPTION

Gas adsorption is an important method to characterize structural features of porous solids and gives information about a pore volume, pore size, pore size/volume distributions and specific surface area of the material. Depending on the nature of the material and information required different probe gases like N_2, Ar or Kr can be used. To determine the specific surface area the BET-method, named after the inventors Stephen Brunauer, P.H Emmett and Edward Teller, is by far the one most used.[85] If desorption- and adsorption-data are collected at several points of relative pressure(p/p0) an isotherm can be plotted from which information about micro-, meso-, or macroporosity and pore size distribution can be deduced applying suitable theoretical models to analyze the data.[86]

6. NANOSTRUCTURED SIO_2

6.1. GELATION OF WATERGLASS

A comparison between two routes for gelation of waterglass was made by increasing the concentration or decreasing pH, respectively, to get a deeper understanding of the molecular mechanisms involved in gelation induced by these alterations. Both routes showed coarsely an apparently similar dependence of their respective variables generating a gradually stiffer and jelly-like appearance. However, the properties of the waterglass following the two different routes are quite different on a molecular level, as will be shown here. Both routes result in a dramatically increased viscosity with the range of change studied as seen in Figure 14. With increased silica concentration a continuous increase in viscosity was observed whereas the pH-adjusted series showed almost constant viscosity in the range from pH 11.94-11.31 below which the viscosity increases rapidly. The results are indicative of some kind of gelation or colloidal aggregation behavior.

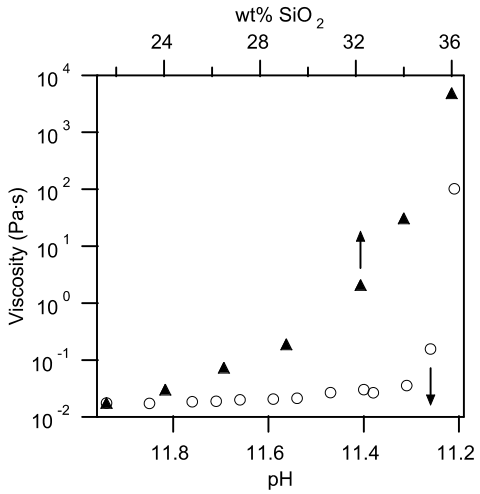

Figure 14. Viscosity of water glass gradually adjusted either by increased silica concentration (full markers) or pH-adjustment (open markers).

The two series of samples were analyzed by ^{29}Si NMR to gain information of the effects of the two variables on the molecular level. The area under the peaks present in the NMR-spectrum (Figure 10) is proportional to the concentration of the particular chemical structure it represents, such as Q^0, Q^1, Q^2 etc. The integral values for the spectral peaks corresponding to Q^0-Q^4 species are plotted as a function of silica concentration and pH, respectively in Figure 15. All data have been normalized so that the total peak area is 100 for each sample. From literature it is suggested that these kinds of concentrated highly alkaline solutions consists of both low molecular weight

species as well as larger particles.[43,53] Also for the ^{29}Si NMR measurements there is a distinction between the two routes. For the samples following the increased silica concentration route the distinction of the different Q-species is almost not affected. But for the pH-adjusted sample series an increase of Q^3 and Q^4 species at the expense of Q^1 and Q^2 species can be seen with decreasing pH..

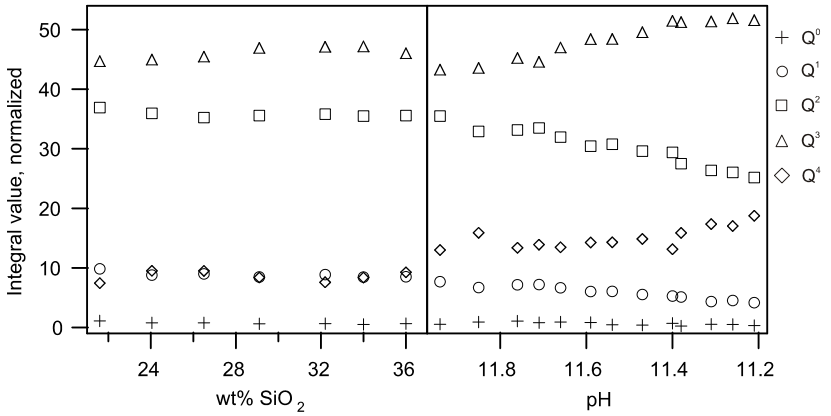

Figure 15. Integral values for the NMR peaks attributed to the different silica species present in waterglass as a function of increased silica concentration (left) or decreasing pH (right). The values are normalized to constant a total integral peak area of 100.

When analyzing the two sample series with dynamic light scattering, two relaxation processes can be distinguished; one fast and one slow (Figures 5 and 8 in Paper I). For the increased silica concentration sample series, the strength of the slow process relative to the fast process increases with increased concentration. This indicates a relative increase in number of large particles compared to low molecular species. The increased viscosity observed with increased silica concentration (Figure 14) is accompanied by an increased relaxation time of the same order of magnitude for the slow process (Figure 6 in Paper I). For the pH adjusted series the relaxation time does not follow the same exponential behavior as the series with increasing silica concentration and the increased relaxation time does not increase with the same order of magnitude (Figure 9 in Paper I). The corresponding particle sizes of the silica species present in the solutions can be calculated from the relaxation measurements (see paper I). For the series with increased silica concentration the large particles decrease from 40 nm to 10 nm as the concentration increases. In contrast for the pH adjusted sample series the large particle size remain essentially constant at 40 nm and almost independent of the decrease in pH. Furthermore changes can be observed by IR-measurements in the amount of Si-O-Si bondings in the waterglass for the pH-adjusted but not for the concentrated sample series (Figure 12 in Paper I).

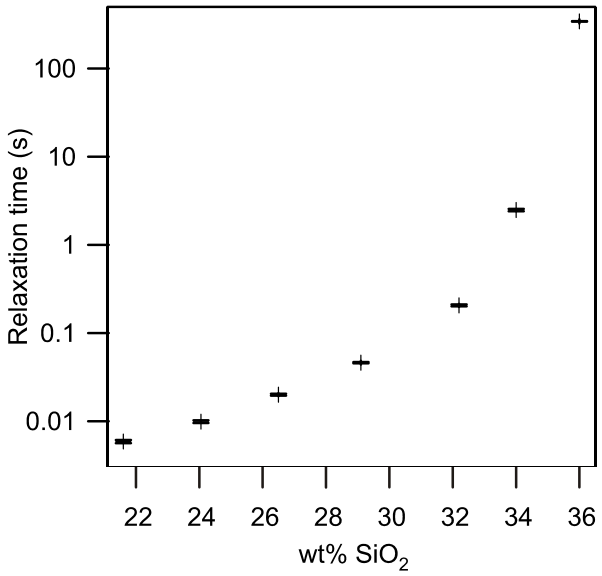

Figure 16. Relaxation times for the slow process of the waterglass as a function of increased silica concentration.

Both NMR-measurements and IR-results show that when the pH is reduced in the waterglass there is an increase in amount of Si-O-Si bonds present due to condensation of the least condensed silica species (Q^0, Q^1 and Q^2) forming more condensed molecular species (Q^3 and Q^4). In agreement with this light scattering data show no size change of the large particles so the results must be due to condensation of low molecular species to larger particles, see Figure 17. Larger clusters or network segments with a rather open non-rigid structure is formed when these species gradually condense. This would explain the sudden increase in viscosity that happens at a critical size where the physical interaction between the particles presumably leads to entanglements.

According to the light scattering data, there is a decrease in particle size for the increased silica concentration series. One could assume that this would lead to an increase in Q-species located at the surface and thus preferentially an increase in Q^3 at the expense of Q^4. However both NMR- and IR-measurements tell us that there is no net transformation of the number of Si-O-Si bonding. This is illustrated by the model in Figure 17. The medium sized particles (10 nm) are formed through a combined process of, dissolution of large particles and a condensation of low molecular species so that the net amount of substitution is close to zero. This apparently contradictory phenomenon is assumed to have its origin in an increased pH and increased concentration due to the loss of water, and the complicated interplay between these two factors and their influence on the equilibrium distribution of silica speciation. Further since this leads to an increased surface area of the larger particles an increased excluded volume for the low molecular species around the larger particles is also expected.

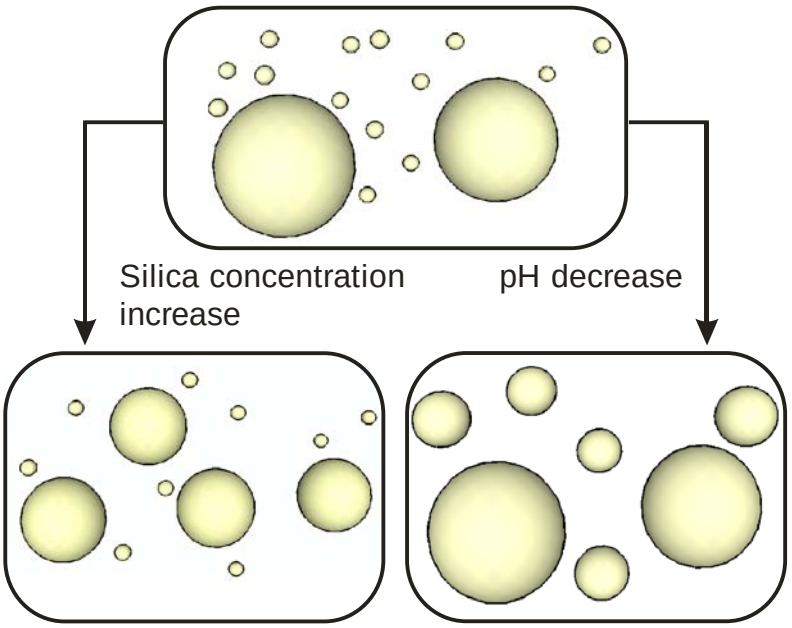

Figure 17. The proposed models for the gelation of waterglass. For the increasingly concentrated waterglass mainly the larger particles are affected whereas the decreased pH leads to increased condensation of the smaller molecular species.

6.2. MESOSTRUCTURED SiO_2 FROM ALKALINE SILICATE SOLUTIONS

Synthesis of mesostructured silica using nonionic surfactants and waterglass is interesting from both environmental and cost reasons. By studying the gelation of waterglass the insight about the chemistry and behavior of waterglass at these alkaline conditions was increased. However, when performing a synthesis of mesostructured silica not only the gelation of silica is important. Three important criteria that need to be considered to make mesoordered silica via liquid crystal templating using nonionic surfactants and waterglass at alkaline conditions have been indentified in this project. These are the silica surfactant interaction, the silica concentration within the liquid crystal, and the gelation and condensation of silica.

6.2.1. INFLUENCE OF SILICA ON SURFACTANT PHASE BEHAVIOR

The nonionic surfactant Brij 56 ($C_{16}EO_{10}$) has previously been successfully used for templating of mesoordered silica using tetramethyl orthosilicate as silica source.[24] Here, a comprehensive study on the influence of silica on the phase behavior of Brij 56 and waterglass was made as a initial step towards a synthesis method using alkaline waterglass and nonionic surfactants. To study the phase behavior small angle X-ray scattering (SAXS) and cross polarized microscopy (CPM) were used. Some of these results are exemplified in Figure 18.

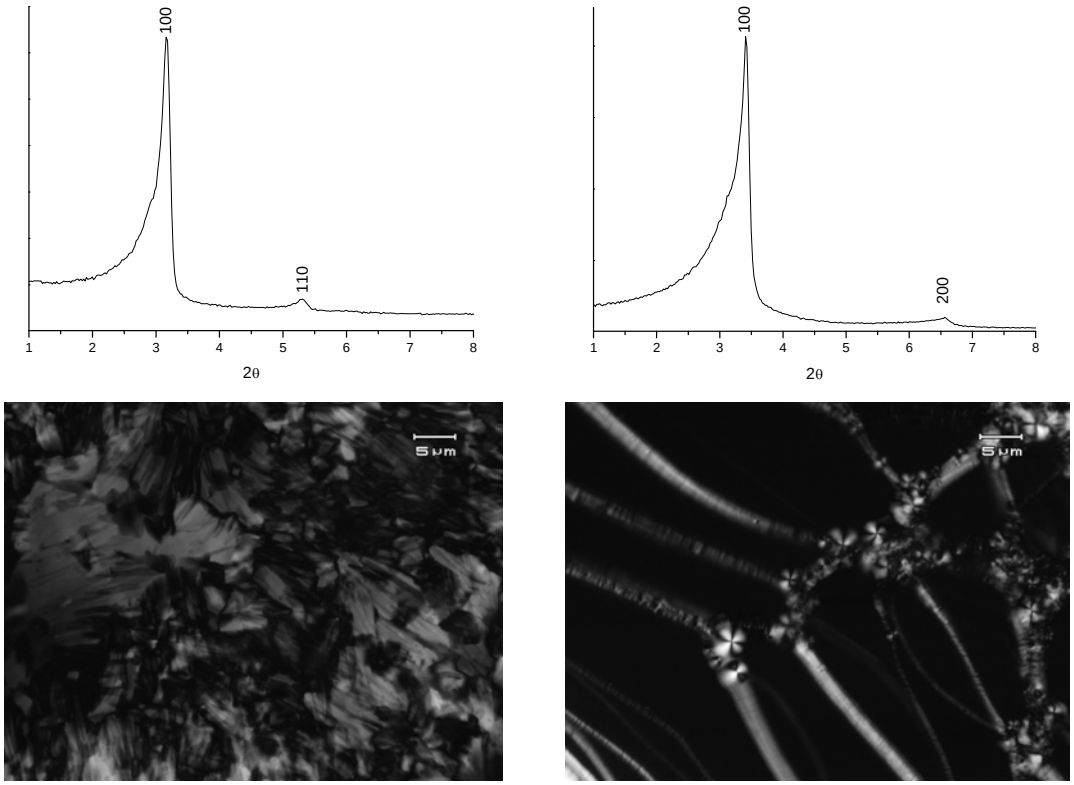

Figure 18. SAXS patterns (top) and CPM-pictures (bottom) of Brij 56 and waterglass mixed in the compositions 30 wt% Brij 56/70 wt% waterglass (left) and 60 wt% Brij 60/40 wt% waterglass (right). Both SAXS and CPM show typical patterns of hexagonal (left) and lamellar (right) structures.

The results of the complete sample series are summarized in Table 1. The phase behavior is affected when using waterglass instead of water and the liquid crystalline phases instead appear at lower surfactant concentrations. This shift shows that the silica-surfactant interaction is somewhat different from the water surfactant interaction, which has previously been attributed to entropic effects for the nonionic block copolymer system at slightly acidic conditions.[87] It was reported that the silica speciation largely affects the interaction between silica and the amphiphile.

Table 1. Phase behavior for mixtures of Brij 56 and water or waterglass (22.5 wt% SiO_2, SiO_2:Na_2O weight ratio~3) respectively. A shift for all phases, hexagonal (hex.), cubic (cub.) and lamellar (lam.) towards lower concentrations is apparent when waterglass is used instead of water.

Composition wt-ratio	20/80	30/70	40/60	50/50	60/40	70/30	80/20
Brij 56/Water	-	-	Hex.	Hex.	Hex.	Cub.	Lam.
Brij 56/Waterglass	-	Hex.	Hex.	Cub.	Lam.	Lam.	Lam.

6.2.2. INFLUENCE OF SILICA CONCENTRATION OF THE WATERGLASS

The silica concentration within the water glass needs to be high enough to create a stable and continuous network within the hydrophilic parts of the liquid crystal to enable formation of a mesostructured silica. From the studies of the concentrated waterglass solutions it was found that the waterglass becomes highly viscous already at silica concentrations around 30 wt%. Creating a liquid crystal by mixing waterglass with surfactant at such conditions was found to be very difficult and unpractical. Therefore the surfactant and the waterglass must be mixed in a first step followed by concentration of silica through evaporation of water in a second step. Following such a procedure, the water was removed through rotary evaporation from a mixture containing 20% Brij 56 and 80% waterglass (24.5 wt% starting concentration of silica). In this way the silica concentration increases simultaneously as the phase shifts from the micellar into the liquid crystalline domains of the phase diagram, as is illustrated by the dotted line in Figure 19.

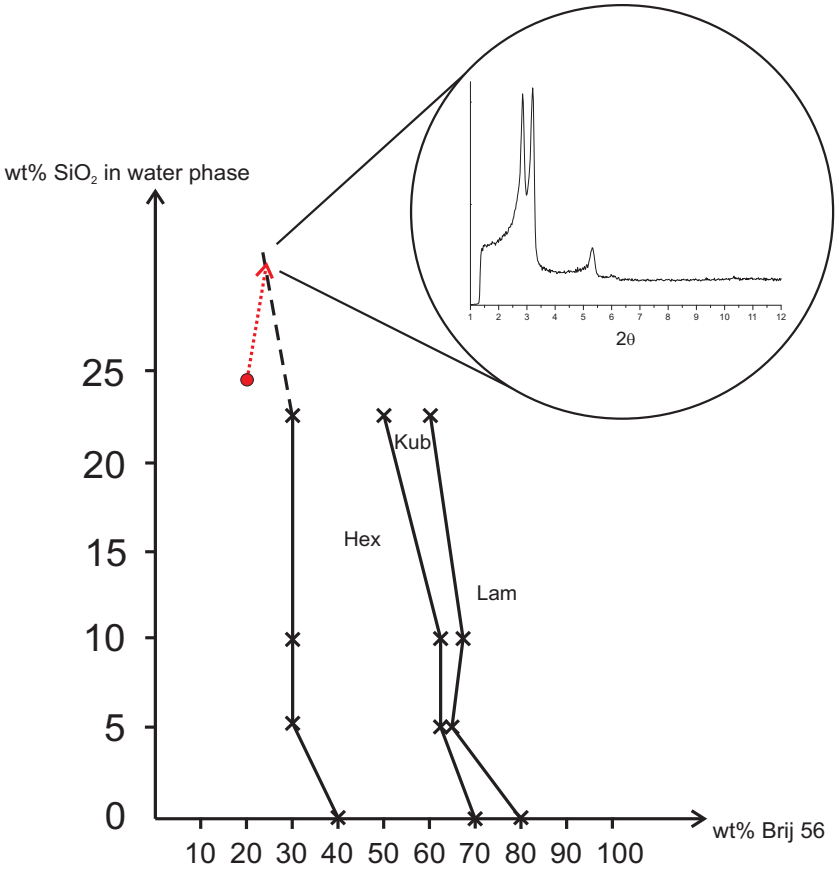

Figure 19. Illustration of the phase dependence Brij 56 upon concentration of silica in the waterglass. The inset shows the SAXS pattern collected on the final mixture obtained after evaporation of solvent following the dotted arrow.

6.2.3. GELATION AND CONDENSATION OF SILICA IN A LIQUID CRYSTAL PHASE

Knowing that liquid crystals can be formed at both low and high silica concentrations is useful, but still the challenge to induce gelation and condensation of the silica monomers in the liquid crystal remains. As described in Section 3.1.1 this can be done either via pH adjustment through addition of acid or using a proton ion exchange resin, or via electrostatic destabilization through salt addition. Several attempts to lower the pH of the waterglass via addition of acid were made but a persistent problem of this approach is the local pH reduction in the solution that causes local formation of insoluble silica precipitates. For waterglass solutions of lower silica:alkali ratio, containing large amounts of reactive silica monomers, this problem becomes even larger. Therefore a combination of the two other methods, ion exchange and salt addition, was evaluated. This time the aqueous part was a waterglass containing 10 wt% silica a SiO_2:Na_2O ratio = 20 and the amphiphile used was the block copolymer pluronic F127. Waterglass of lower concentration and higher silica:alkali consists of a stable suspension of very small colloidal silica particles and the gelation and condensation will thus be easier to control. Pluronic F127 has a phase diagram with water that exhibits large regions of liquid crystalline phases that form at room temperature, which makes it easier to work with compared to Brij 56. By using a waterglass solution with a high silica/alkali-ratio the pH adjustment as well as the gelation through salt addition could be satisfactory controlled.

Table 2. Sample solutions with salt- and surfactant-content displayed

Sample	$[NaCl]_{reaction\ solution}$ mol/L	$[F127]_{reaction\ solution}$ wt%
A1	0.05	0
A2	0.1	0
A3	0.15	0
A4	0.2	0
B1	0.05	15
B2	0.1	15

A series of waterglass solutions at pH 8, A1-A4 Table 2 were prepared to evaluate how the gelation rate is affected by the salt concentration. The four solutions A1-A4, containing no surfactant, show an exponential trend in gelation time with decreasing salt concentration shown in Figure 20.

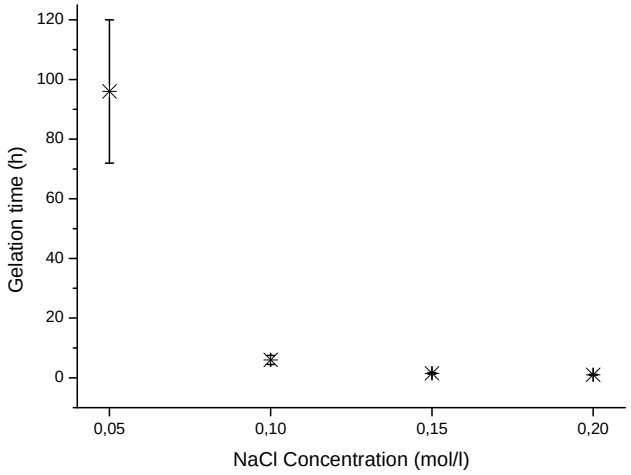

Figure 20. Gelation time for waterglass solutions containing 10 wt% silica at pH 8 with varying amounts of added salt.

In the syntheses performed following this method the ion exchange resin was added to the waterglass solution, the mixture stirred until the pH reached 8 at which point the ion exchange resin was removed from the mixture. From this batch two waterglass solutions, B1 and B2 containing 0.05 and 0.1 M NaCl and 15wt% pluronic F127 were prepared as described in Table 2. The reaction solutions were then poured into petridishes and aged while letting most of the water evaporate. The final products were calcined to remove the amphiphilic template and form mesoporous solids.

The porosity of samples B1 and B2 was evaluated using N_2 gasadsorption and TEM and compared with the corresponding samples prepared without surfactant, A1 and A2. The gas adsorption results are shown in Figure 21. With the isotherms shown in the inset showing adsorption behavior similar to type IV physisorption isotherms which according to IUPAC definition is associated with capillary condensation taking place in mesopores.[86] The TEM micrographs that were collected on the A- and B-samples were not able to depict these differences. However this is not so surprising since the pore size distributions of the samples are relatively broad and to some extent also overlap between the samples. Therefore the TEM-micrographs might appear similar even though the larger poresize of the A-samples is evident from the gas-adsorption measurements.

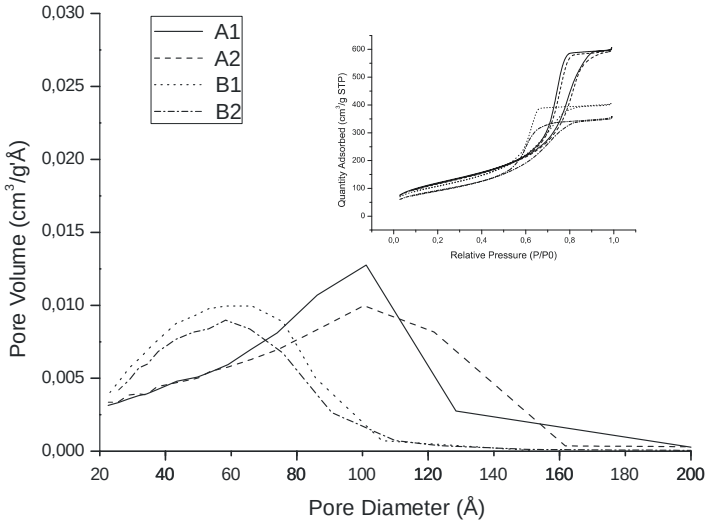

Figure 21. BJH pore size distributions derived from the adsorption branch of the isotherms (inset) of samples with and without surfactants.

6.2.4. INFLUENCE OF THE SILICA:ALKALI RATIO OF THE WATERGLASS

As already mentioned, the gelation of waterglass with high silica:alkali ratio is easier to control compared to waterglass with low silica:alkali ratio because of lower reactivity. But high ratio also means the waterglass to a higher extent consist of large colloidal particles.[88] Depending on the size these particles can be hard to include in a mesoordered pore wall. To get round this problem a low silica:alkali ratio waterglass (SiO_2:Na_2O=3) with a silica concentration of only 5 wt% was used. To induce gelation in this waterglass addition of extra salt was not needed because of the already high alkali concentration. The pH of this waterglass solution was adjusted to pH 8; and the block-copolymer, pluronic F127 was added so that the final composition contained 5 wt% F127. The mixture was then spincoated on substrates and the mesostructured was formed according to the EISA method.[26] When the water evaporates the concentration of the silica increases and the mixture transferred into the liquid crystalline area of the phase diagram. A TEM micrograph of the material thus prepared and after subsequent removal of the polymer template is shown in Figure 22. It can clearly be seen that an ordered mesoporous structure has been achieved. To the best of our knowledge, this is the first example of an ordered mesoporous silica prepared using nonionic amphiphile and alkaline water glass as silica source.

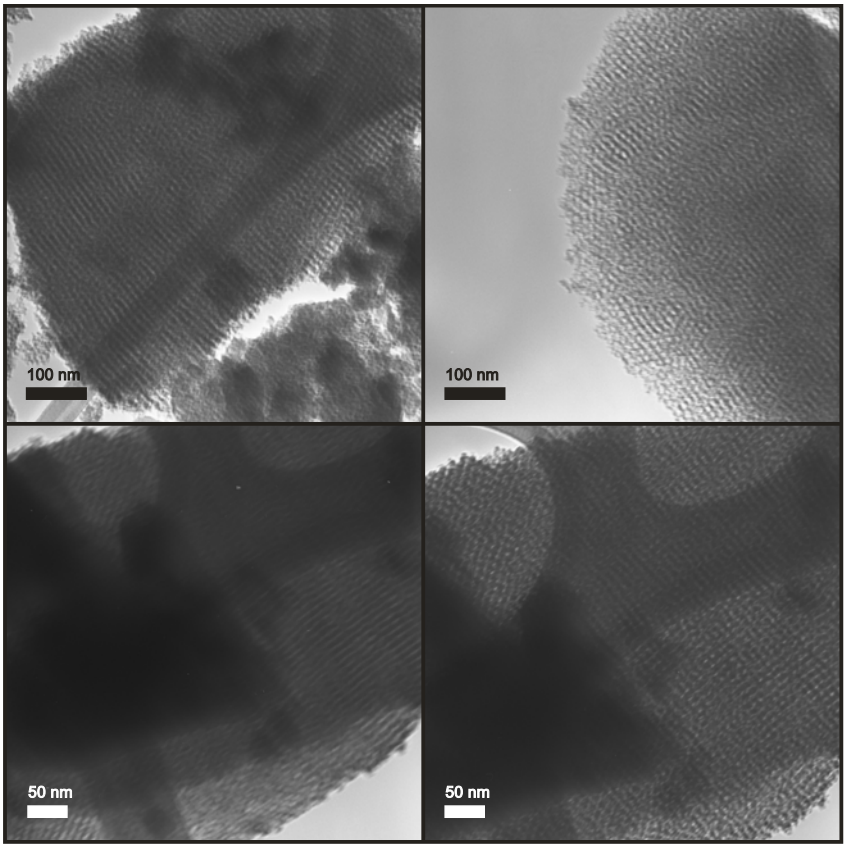

Figure 22. TEM micrographs of the calcined sample prepared by spincoating of a waterglass-solution (5 wt-% SiO_2 and SiO_2:Na_2O weight ratio~3) containing 5 wt% F127.

7. NANOSTRUCTURED TIO2

7.1. MICROEMULSION SYNTHESIS OF TIO_2 CRYSTALLITES

Several methods for preparation of nanoparticulate materials, both at very high temperatures[89-91] as well as low temperature solution-based methods[72,92] are being developed. The solution based-methods generally have a slower synthesis path, however the potential of making new kinds of materials through the interaction with surfactants in solution makes them interesting.

The phase behavior of surfactant solutions are temperature sensitive and the reaction must therefore be performed at low temperatures. This means that crystallization of the desired polymorph also has to take place at lower temperatures. Microemulsion synthesis at room temperature has been performed by Andersson et al. using the nonionic surfactant Triton X-100.[92] In that study it was shown that microemulsions may be used to enable formation of rutile at room temperature, which typically requires high temperature treatments for formation through solid state synthesis procedures. Inspired by this work a new low-temperature microemulsion synthesis based on the block copolymer pluronic F127 has been developed in paper III. $Pluronics_{(TM)}$ is the trade name of a group of surface active block copolymers, build up by ethyleneoxide- and propyleneoxide-blocks. A three phase system composed of pluronic F127, butanol and water, was published by Holmqvist et. al[93] and is reproduced in Figure 23.

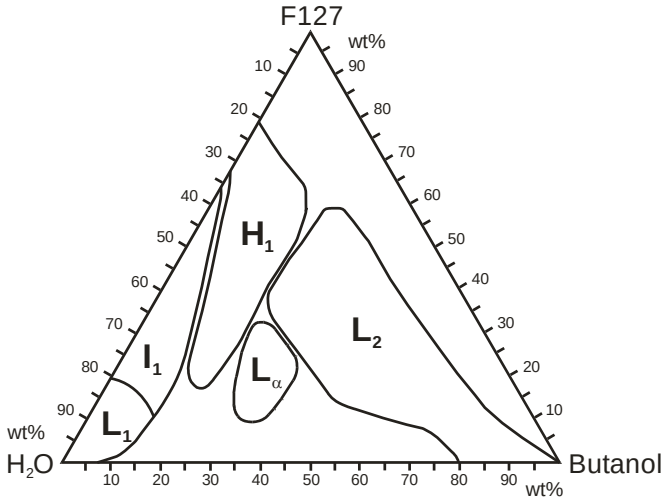

Figure 23. Phase diagram of H_2O/butanol/F127 redrawn from Holmqvist et al.[93]

The pluronic F127 phase diagram contains large areas of liquid crystalline phases which have been used extensively as templates for the formation of mesoordered materials. The results of the

pluronic F127 microemulsion-based synthesis performed at different temperatures are presented in Figure 24.

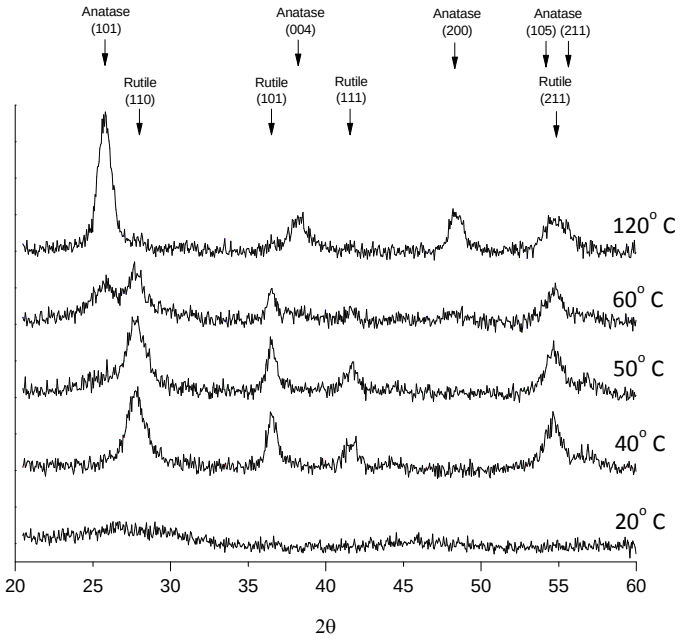

Figure 24. Powder X-ray diffractograms of materials formed during 96h of synthesis in 5M HCl made at different temperatures.

In contrast to similar synthesis conditions using triton X-100 where rutile was formed[92], the product formed in the pluronic F127 system remains amorphous at 20° C even after 4 days. However, if the synthesis is performed at 40° or 50° C, rutile is formed. For syntheses at 120 ° C anatase is kinetically favored in agreement with the synthesis made with Triton X-100[92] whereas at 60 ° C there is a coexistence of rutile and anatase. Figure 25 shows how the composition at 60 ° C changes with synthesis time.

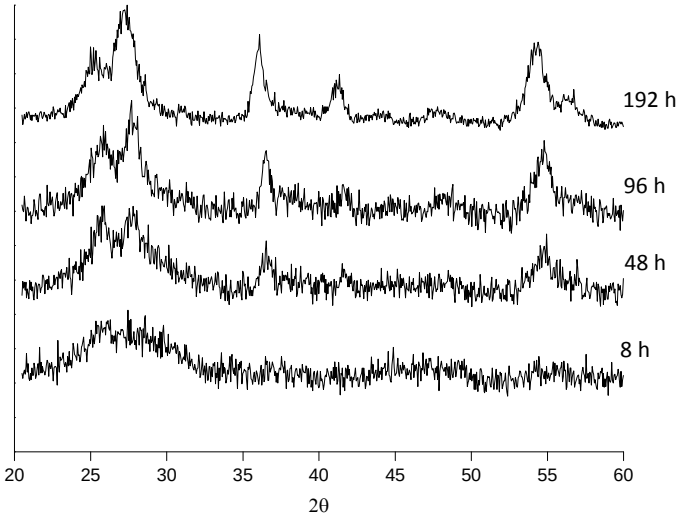

Figure 25. Powder x-ray diffractograms of materials formed at 60° C of synthesis in 5M HCl made at different synthesis time periods.

In contrast to the samples made at hydrothermal conditions it seems from these results that a transformation from anatase to rutile happens at prolonged synthesis time periods. The exact composition is listed in Table 3.

Table 3. Polymorph composition of materials formed at 60° C of synthesis in 5M HCl made at different synthesis time periods.

	Synthesis time			
	8h	48h	96h	192h
Rutile (%)	22	54	58	71
Anatase (%)	78	46	42	29

Not only time and temperature are important factors for the crystallization of titania. Figure 26 illustrates how the crystallinity is affected by the choice of acid used. It is clear from this figure that the strength of the acid is not as important as the type of acid used. Apart from a small shoulder at the anatase (101) position for the lowest hydrochloric acid concentration the only difference is seen when switching between hydrochloric acid and nitric acid. Most materials prepared have a specific surface area much below 100 m^2/g, except for the materials prepared at hydrothermal conditions which showed a specific surface area close to 200 m^2/g. The measured low specific surface area is likely due to that the crystals formed associate in-needle shaped aggregates, which are arranged in bundles as can be seen from the TEM micrograph in Figure 27 and that the pores of these aggregates possibly do not allow for adsorption of nitrogen molecules.

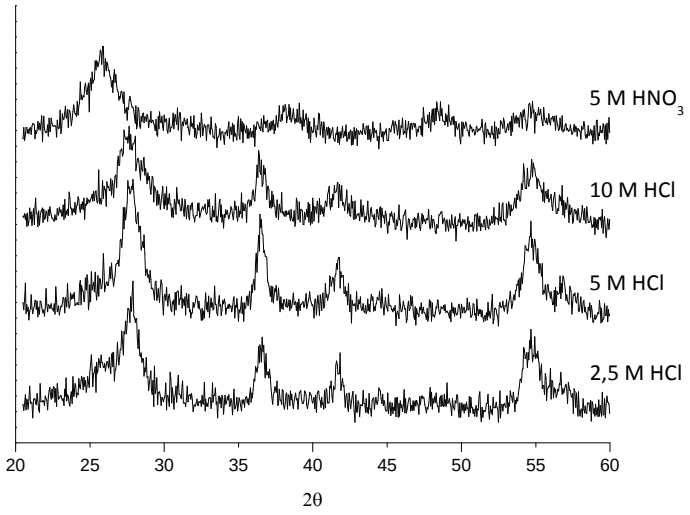

Figure 26. Powder X-ray diffractograms of materials prepared during 96h of synthesis using different acids at 50° C.

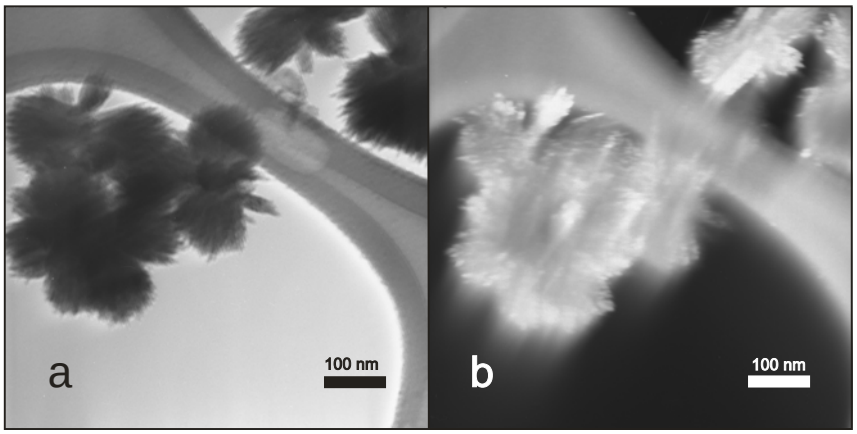

Figure 27. TEM bright field image (a) and dark field image (b) of materials prepared during 96h of synthesis using 5M HCl at 50° C showing typical appearance of needle shaped crystallites arranged in bundles.

Under synthesis conditions the rate of nucleation and crystal growth of the particles depend on both molar compositions and temperature used. This will likely affect the rate determining energies involved in the different reaction steps, why the interplay between thermodynamics and formation kinetics result in polymorphs that *a priori* may be expected to be less favored. The surfactants triton X-100 and pluronic F127 are very different in molecular size and structure why also the colloidal stabilization and particle aggregation properties appear different. These differences between the two amphiphiles are also expected to result in different dynamics and reaction kinetics of the two systems.

7.2. MESOORDERED CRYSTALLINE TIO_2

The inhibition of electron hole recombination is an important key to improve the photocatalytic activity of a photocatalyst as previously discussed. Potentially this property may be improved with a mesoporous material, which may enhance the transportation of electrons to the surface so that reaction can take place before electrons holes recombine. The most obvious advantage, however, of a mesoporous titania is its larger specific surface area and thereby the contact with the reactants. The fact that crystalline titania nanoparticles can be nucleated and grown in a pluronic-based microemulsion at low temperatures opens the door for liquid-crystal templating of these crystallites into mesoorded arrangements.[94] As can be seen in Figure 23 hexagonal (H_1) as well as cubic (I_1) phases exist over a wide area of the phase diagram.

7.2.1. SYNTHESIS METHOD

Since the synthesis of the titania nanocrystallites is performed within the reversed micellar area (L_2) of the phase diagram the phase composition needs to be shifted into the liquid crystal area during the synthesis to enable mesostructuring. A schematic description of the synthesis is given in Figure 28. The synthesis of mesostructured titania with nanocrystals constituting the walls is performed in three stages starting with nucleation and growth of crystallites in the microemulsion-based nanocrystal formation step. By varying the synthesis time of the crystals their size can be tuned (stage 1). After this stage the reaction solution is spin coated onto a substrate. Evaporation of the solvent shifts the phase conditions into the liquid crystal phase with the crystallites included (stage 2). In the last step of the synthesis the liquid crystal template is removed by UV-irradiation (stage 3) leaving the ordered mesoporous and crystalline titania.

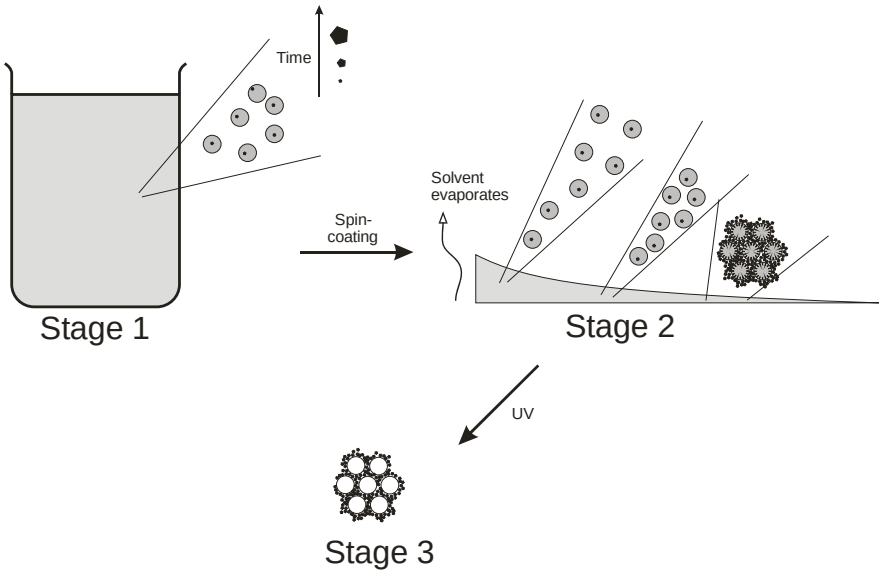

Figure 28. Synthesis of mesoordered anatase

7.2.2. CHARACTERISATION OF MESOORDER

As described, the crystalline nanoparticles form in the first stage of the synthesis and are then incorporated in the pore wall of the material through the coassembly process with the block copolymer forming the liquid crystal. The crystallite size is a limiting factor for the mesoorder. At certain synthesis time the crystallites will have grown too large to fit within the pore walls of the structure whereby the mesoorder will be lost. The samples were spin coated from the microemulsion solution at 3, 6, 12, 24 and 48 hours of nanocrystal synthesis time. High resolution transmission electron microscopy was used to characterize the materials and the results for samples made between 3-24 hours are shown in Figure 29. A hexagonal arrangement of the materials is clearly seen in images (a-d). However, at 24 hours the order becomes distorted and at 48 hours the long range order is almost completely lost. With higher resolution, the crystal fringes become apparent in the pore walls in images (e-h).

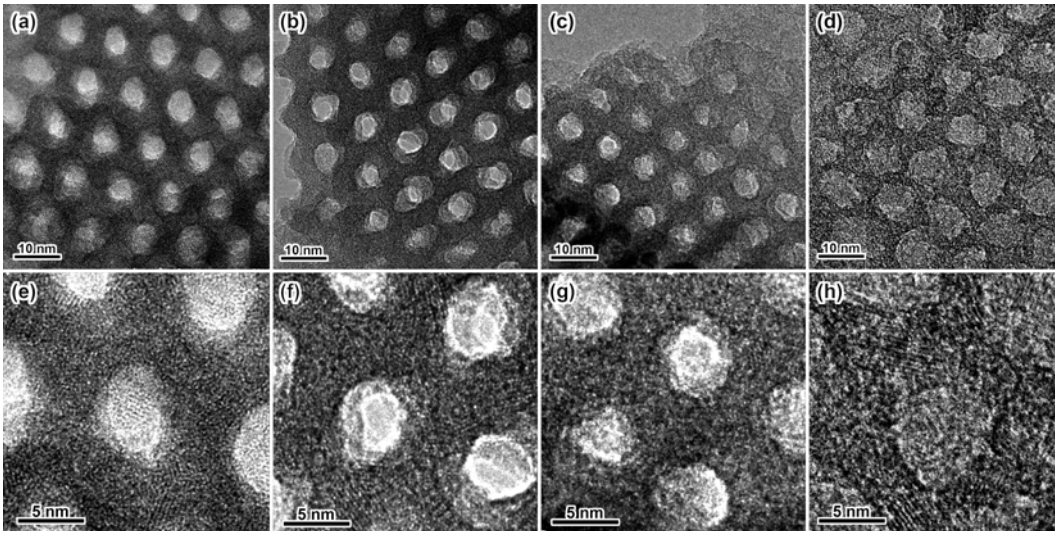

Figure 29. High-resolution TEM images of mesoporous TiO_2 prepared at different reaction times ranging from 3 hours (a, e), 6 hours (b, f), 12 hours (c, g) to 24 hours (d, h). Images (e-h) show the magnified images of TEM images (a-d), illustrating the effects of synthesis time on mesostructured.

7.2.3. CHARACTERISATION OF ATOMIC ORDER

Electron diffraction (ED) analysis was used to characterize the atomic order of the crystallites. The ED-patterns and the bright field images images for syntheses made at 3, 12 and 48 hours are shown in Figure 30. Gold sputtered grids were used as an internal standard to calibrate the camera length. For characterization of the atomic order the rotational averages of the Debye-Scherrer rings were collected.

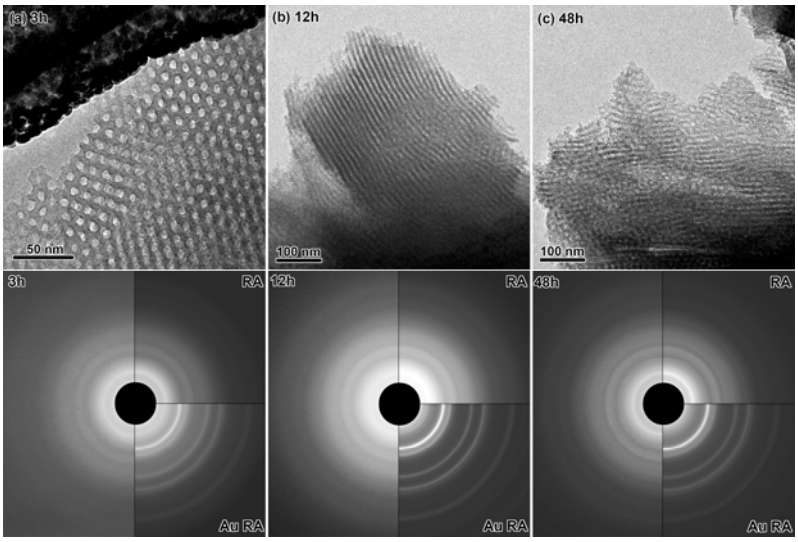

Figure 30. Low magnification TEM images of mesoporous TiO_2 prepared at different reaction times. The bottom part shows the electron diffraction (ED) patterns of each sample divided in three parts. Images show ED patterns (left) and rotational averaged ED patterns (right-top) of the mesoporous TiO_2, and the rotational averaged ED patterns of sputtered gold for calibration (right-bottom).

In Figure 31 the intensity profile of the rotational average Debye-Scherrer rings is plotted versus the inverse of the d-spacing of the characterized materials. All materials show an intensity profile that corresponds better to anatase than rutile or brookite. The peaks are, not surprisingly, stronger for the 48 hour sample but they are clear also for the two samples made at shorter synthesis times. The first peak, which is present around 1/d=2,9 nm^{-1} is assigned to the (101) reflection of the anatase structure, which is the strongest reflection for anatase.

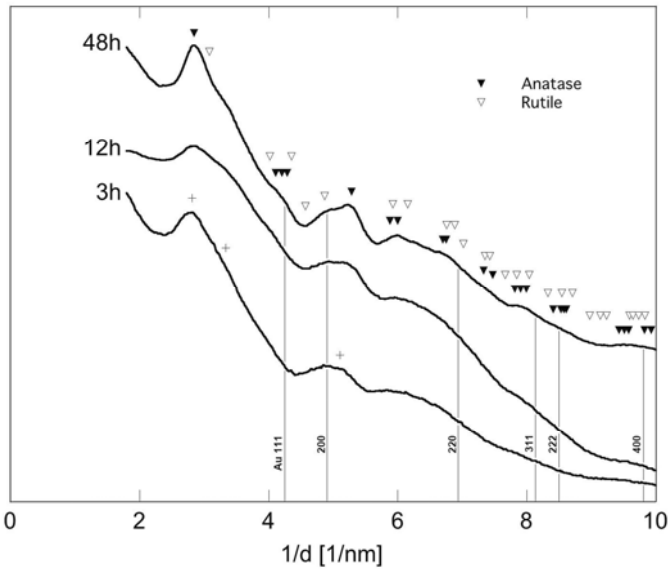

Figure 31. The intensity profile of the rotational average ED-patterns prepared at 3, 12 and 48 hours.

The synthesized mesoordered titania was evaluated for the use in dye-sensitized solar cells. A dye denoted D6 was used as sensitizer. The structural formula for this dye is given in Figure 32. The mesoporous TiO_2 materials were applied to a DSSC cell either as prepared or following a heat-treatment at 450° C for 2 hours. For some applications, such as solar cells applications thermal pre-treatment of the mesoporous TiO_2 material might be necessary. It was found during the heat treatment that the mesoporous material prepared here has a very high thermal stability compared to similar materials prepared with other methods.[32,33] Thus the mesoorder remains intact after heat treatments at 450° C as shown in Figure 33. This may be due to lower degree of stresses in the material prepared by ready-made nanocrystallites compared to materials prepared via solid state crystallization of amorphous material ordered in a mesostructure.

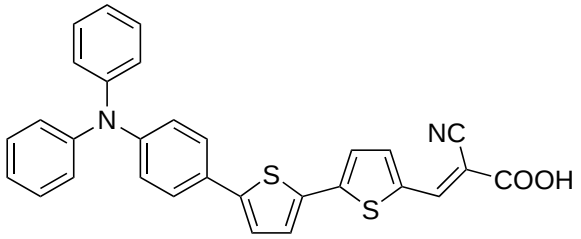

Figure 32. The structural formula for the dye D6 used as sensitizer in the DSSC tests. The chemical formula is 2-cyano-3-(5´-(4-(diphenylamino)phenyl)-[2,2´-bithiophen]-5-yl)acrylic acid.

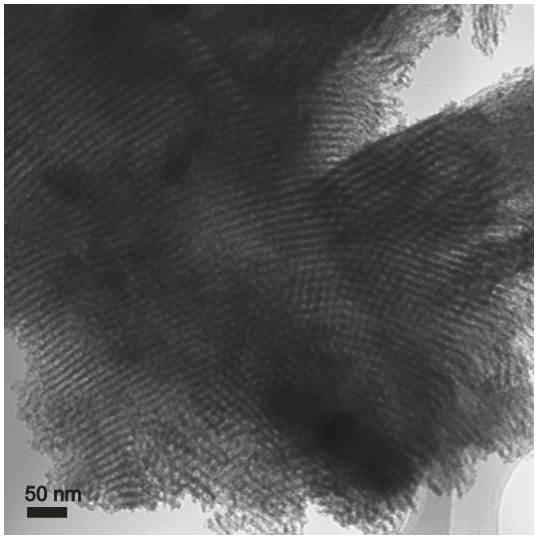

Figure 33. Mesoporous TiO_2 prepared after synthesis time of 12 hours, followed by heat treatment of as prepared mesoporous TiO_2 at 450° C for 2 hours to condition it for DSSC tests.

The DSSC measurements were carried out at a light intensity of 1 sun (1000W/m^2). The preliminary results of efficiency are plotted in Figure 34. The materials are thus shown to work as electrode for DSSC but the efficiency obtained is relatively low compared to a normal

nanoporous TiO_2 electrode. This could possibly be due to a lower amount of dye possible to introduce to the surface of the TiO_2 compared to ordinary nanoporous TiO_2 due to more narrow pore size or different surface characteristics. The heat-treatment of the samples has a strong effect and increases the efficiency roughly by a factor of 8. Plausible explanations for this is an increased connectivity between the particles because of the sintering and an increased degree of crystallinity.

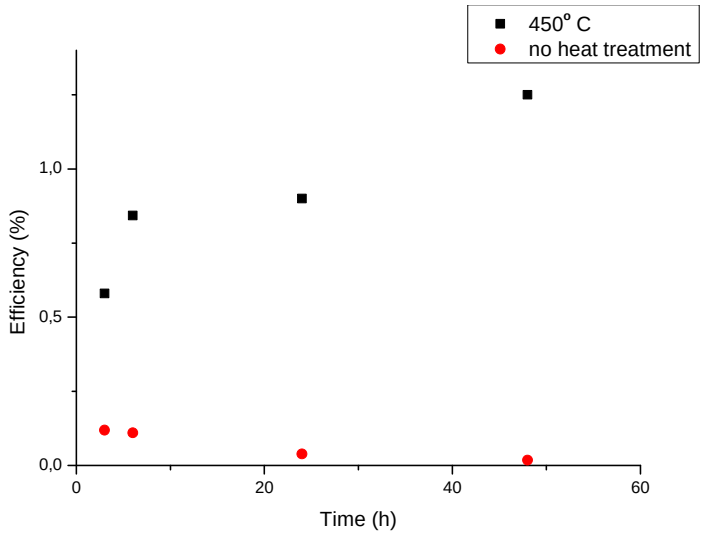

Figure 34. DSSC efficiency plot for the mesoporous TiO_2 series with and without heat treatment at 450° C prior to dye incorporation.

8. CONCLUDING REMARKS

The silica project reported here started with the original idea to develop a new method to make mesoordered silica from waterglass based on direct templating. The approach seemed simple enough and would be straight forward and low cost which made it very interesting. However, when it comes to research, simple ideas are often more challenging than they first appear. The key to solve we soon realized was to find a controlled way to induce the gelation and condensation of the silica monomers within the liquid crystal. When looking in to this issue the behavior of the waterglass caught our interest and a study of the gelation behavior was initiated to deepen the understanding of waterglass at high concentration and pH. The focus of the project was thereafter changed from a direct templating synthesis to a synthesis at alkaline conditions still using waterglass as the silica precursor and nonionic surfactants as structure directing agent.

In parallel with the silica studies a second project, focusing on mesoordered synthesis of crystalline titania was conducted. The primary idea was to incorporate nanoparticulate crystalline titania in a mesoordered structure via liquid crystal templating. The liquid crystals do not exist at temperatures where titania normally crystallizes through solid state reaction. Earlier work had shown that low temperature microemulsion synthesis of crystalline titania was possible. However, this synthesis was made in systems that suffered from lack of easily accessible liquid crystalline phases. Therefore the first aim was to find new conditions for low temperature synthesis of crystalline nanoparticulate titania in an amphiphilic system which also had high potential for liquid crystal templating. Following this development the second step was taken which enabled a new method for low temperature synthesis of crystalline titania in an ordered mesoporous structure was developed.

Lot of knowledge has been conquered personally by the author while working on this thesis and it is the author's wish that some of it also will become useful for other researchers.

REFERENCES

1. Rouquerol, J. et al. *Pure Appl. Chem.* 66 (8), 1739-1758 (1994).
2. Yanagisawa, T., Shimizu, T., Kuroda, K., & Kato, C. *Bull. Chem. Soc. Jpn.* 63 (4), 988-992 (1990).
3. Inagaki, S., Fukushima, Y., & Kuroda, K. *J. Chem. Soc. Chem. Commun.* (8), 680-682 (1993).
4. Kresge, C.T., Leonowicz, M.E., Roth, W.J., Vartuli, J.C., & Beck, J.S. *Nature* 359 (6397), 710-712 (1992).
5. Beck, J.S. et al. *J. Am. Chem. Soc.* 114 (27), 10834-10843 (1992).
6. Berggren, A., Palmqvist, A. E. C., Holmberg, K. *Soft Matter* 1, 219-226 (2005).
7. Palmqvist, A.E.C. *Curr. Opin. Colloid Interface Sci.* 8, 145-155 (2003).
8. Holmberg, K. *J. Colloid Interface Sci.* 274, 355-364 (2004).
9. Beck, J.S. & Vartuli, J.C. *Curr Opin Solid State Mater Sci* 1 (1), 76-87 (1996).
10. Carreon, M.A. & Guliants, V.V. *Eur. J. Inorg. Chem.* (1), 27-43 (2005).
11. Wan, Y., Shi, Y.F., & Zhao, D.Y. *Chem. Commun.* (9), 897-926 (2007).
12. Sayari, A. & Liu, P. *Microporous Mater.* 12 (4-6), 149-177 (1997).
13. Soler-illia, G.J.D., Sanchez, C., Lebeau, B., & Patarin, J. *Chem. Rev.* 102 (11), 4093-4138 (2002).
14. Zhao, D.Y. et al. *Science* 279 (5350), 548-552 (1998).
15. Yang, P.D., Zhao, D.Y., Margolese, D.I., Chmelka, B.F., & Stucky, G.D. *Nature* 396 (6707), 152-155 (1998).
16. Antonelli, D.M. & Ying, J.Y. *Chem. Mater.* 8 (4), 874-881 (1996).
17. Doi, T. & Miyake, T. *Chem. Commun.* (14), 1635-1636 (1996).
18. Liu, P., Liu, J., & Sayari, A. *Chem. Commun.* (6), 577-578 (1997).
19. Tian, Z.R. et al. *Science* 276 (5314), 926-930 (1997).
20. Templin, M. et al. *Science* 278 (5344), 1795-1798 (1997).
21. Ulagappan, N. & Rao, C.N.R. *Chem. Commun.* (14), 1685-1686 (1996).
22. Choi, M. et al. *Nat. Mater.* 5 (9), 718-723 (2006).
23. Zhao, D.Y., Huo, Q.S., Feng, J.L., Chmelka, B.F., & Stucky, G.D. *J. Am. Chem. Soc.* 120, 6024-6036 (1998).
24. Attard, G.S., Glyde, J. C., Göltner, C. G. *Nature* 378, 366-368 (1995).
25. Attard, G.S. et al. *Science* 278 (5339), 838-840 (1997).
26. Brinker, C.J., Lu, Y., Sellinger, A., Fan, H.,. *Adv. Mater.* 11 (7), 579-585 (1999).
27. Corma, A. *Chem. Rev.* 97 (6), 2373-2419 (1997).
28. Chen, L.H. et al. *J. Mater. Chem.* 19 (14), 2013-2017 (2009).
29. Izquierdo-Barba, I., Martinez, A., Doadrio, A.L., Perez-Pariente, J., & Vallet-Regi, M. *Eur. J. Pharm. Sci.* 26 (5), 365-373 (2005).
30. Mangrulkar, P.A., Kamble, S.P., Meshram, J., & Rayalu, S.S. *J. Hazard. Mater.* 160 (2-3), 414-421 (2008).
31. Antonelli, D.M. & Ying, J.Y. *Angew. Chem., Int. Ed.* 34 (18), 2014-2017 (1995).
32. Alberius, P.C.A. et al. *Chem. Mater.* 14, 3284-3294 (2002).
33. Andersson, M., Birkedal, H., Franklin, N.R., Ostomel, T., Boettcher, S., Palmqvist, A.E.C., Stucky, G.D. *Chem. Mater.* 17, 1409-1415 (2005).
34. Grosso, D. et al. *Nat. Mater.* 3 (11), 787-792 (2004).
35. Luchian, C. et al. *Rev. Chim.* 62 (3), 287-292 (2011).
36. Thirumavalavan, M., Wang, Y.T., Lin, L.C., & Lee, J.F. *J. Phys. Chem. C* 115 (16), 8165-8174 (2011).
37. Trejda, M., Stawicka, K., & Ziolek, M. *Appl. Catal., B* 103 (3-4), 404-412 (2011).
38. Vartuli, J.C. et al. *Chem. Mater.* 6 (12), 2317-2326 (1994).
39. Berggren, A. & Palmqvist, A.E.C. *J. Phys. Chem. C* 112 (3), 732-737 (2008).
40. Kim, S.S., Karkamkar, A., Pinnavaia, T.J., Kruk, M., & Jaroniec, M. *J. Phys. Chem. B* 105 (32), 7663-7670 (2001).
41. Coleman, N.R.B., Attard, G. S. . *Microporous and Mesoporous Materials* 44-45, 73-80 (2000).
42. Frasch, J., Lebeau, B., Soulard, M., Patarin, J., & Zana, R. *Langmuir* 16 (23), 9049-9057 (2000).
43. Iler, R.K., *The Chemistry of Silica - solubility, polymerisation, colloid and surface properties, and biochemistry.* (John Wiley & Sons, 1979).

44. Weldes, H.H., Lange, K.R.,. *Industrial and Engeineering chemistry* 61, 29-44 (1969).
45. Munz, K.H. & Sonnleitner, R. *Journal of the American Leather Chemists Association* 100 (2), 66-75 (2005).
46. Soluble Silicates – Chemical, Toxicological, Ecological and Legal Aspects of Production, Transport, Handling and Application Centre Européen d'Etude des Silicates Technical Report, 2008.
47. DN (TT-AFP-Reuters) *Radioaktiv läcka stoppad i Fukushima* Stockholm 2011-04-06 http://www.dn.se/nyheter/varlden/radioaktiv-lacka-stoppad-i-fukushima
48. Kim, S.S., Pauly, T.R., & Pinnavaia, T.J. *Chem. Commun.* (17), 1661-1662 (2000).
49. Kim, J.M. & Stucky, G.D. *Chem. Commun.* (13), 1159-1160 (2000).
50. Harris, R.K., Bahlmann, E.K.F., Metcalfe, K., & Smith, E.G. *Magn. Reson. Chem.* 31 (8), 743-747 (1993).
51. Svensson, I.L., Sjoberg, S., & Ohman, L.O. *J. Chem. Soc., Faraday Trans. I* 82, 3635-3646 (1986).
52. Engelhardt, G., Zeigan, D., Jancke, H., Hoebbel, D., & Wieker, W. *Z. Anorg. Allg. Chem.* 418 (1), 17-28 (1975).
53. Nauman, R.V. & Debye, P. *J Phys Colloid Chem* 55 (1), 1-9 (1951).
54. Marsmann, H.C. *Z. Naturforsch., B: J. Chem. Sci* B 29 (7-8), 495-499 (1974).
55. Yu, J.G. et al. *J. Catal.* 217 (1), 69-78 (2003).
56. Yu, J.G., Yu, J.C., Cheng, B., Hark, S.K., & Iu, K. *J. Solid State Chem.* 174 (2), 372-380 (2003).
57. Fujishima, A. & Honda, K. *Nature* 238 (5358), 37-38 (1972).
58. Hoffmann, M.R., Martin, S.T., Choi, W.Y., & Bahnemann, D.W. *Chem. Rev.* 95 (1), 69-96 (1995).
59. Fujishima, A., Rao, T. N., Tryk, D.A. *J. Photochem. Photobiol. C* 1, 1-21 (2000).
60. Chae, S.Y. et al. *Chem. Mater.* 15 (17), 3326-3331 (2003).
61. Bessekhouad, Y., Robert, D., Weber, J.V., & Chaoui, N. *J. Photochem. Photobiol., A* 167 (1), 49-57 (2004).
62. Li, F.B., Li, X.Z., & Hou, M.F. *Appl. Catal., B* 48 (3), 185-194 (2004).
63. Chen, X. & Mao, S.S. *Chem. Rev.* 107 (7), 2891-2959 (2007).
64. Malato, S., Blanco, J., Vidal, A., & Richter, C. *Appl. Catal., B* 37 (1), 1-15 (2002).
65. Kikuchi, Y., Sunada, K., Iyoda, T., Hashimoto, K., & Fujishima, A. *J. Photochem. Photobiol., A* 106 (1-3), 51-56 (1997).
66. Joo, J. et al. *J. Phys. Chem. B* 109 (32), 15297-15302 (2005).
67. Joo, H.C., Lim, Y.J., Kim, M.J., Kwon, H.B., & Han, J.H. *Appl. Surf. Sci.* 257 (3), 741-746 (2010).
68. Yu, J.C., Yu, J.G., Ho, W.K., & Zhang, L.Z. *Chem. Commun.* (19), 1942-1943 (2001).
69. Li, Y.Z., Lee, N.H., Lee, E.G., Song, J.S., & Kim, S.J. *Chem. Phys. Lett.* 389, 124-128 (2004).
70. Kim, S.J., Lee, H.G., Kim, S.J., Lee, J.K., & Lee, E.G. *Appl. Catal., A* 242 (1), 89-99 (2003).
71. Sun, J., Gao, L., & Zhang, Q.H. *J. Am. Ceram. Soc.* 86 (10), 1677-1682 (2003).
72. Andersson, M., Österlund, L., Ljungstrom, S., & Palmqvist, A. *J. Phys. Chem. B* 106, 10674-10679 (2002).
73. Oregan, B. & Grätzel, M. *Nature* 353 (6346), 737-740 (1991).
74. Hagfeldt, A., Boschloo, G., Sun, L.C., Kloo, L., & Pettersson, H. *Chem. Rev.* 110 (11), 6595-6663 (2010).
75. Grätzel, M., Durrant, J.R., *Nanostructured and photoelectrochemical systems for solar photon conversion*. (Worldscientific, 2008).
76. Canet, D., *Nuclear Magnetic Resonance - Concepts and Methods*. (John Wiley & Sons, Inc., 1996).
77. Harris, R.K. & Knight, C.T.G. *J. Chem. Soc., Faraday Trans. 2* 79 (10), 1525-1538 (1983).
78. Harris, R.K. & Knight, C.T.G. *J. Mol. Struct.* 78 (3-4), 273-278 (1982).
79. Harris, R.K. & Knight, C.T.G. *J. Chem. Soc., Faraday Trans. 2* 79 (10), 1539-1561 (1983).
80. Cho, H. et al. *J. Am. Chem. Soc.* 128 (7), 2324-2335 (2006).
81. Iwamoto, T., Morita, K., & Mackenzie, J.D. *Journal of Non-Crystalline Solids* 159 (1-2), 65-72 (1993).
82. Moravetski, V., Hill, J.R., Eichler, U., Cheetham, A.K., & Sauer, J. *Journal of the American Chemical Society* 118 (51), 13015-13020 (1996).
83. Scherrer, P. *Göttinger Nachricten* 2, 98 (1918).
84. Patterson, A.L. *Phys. Rev.* 56, 978-982 (1939).
85. Brunauer, S., Emmett, P.H., & Teller, E.J. *J. Am. Chem. Soc.* 60 (2), 309-319 (1938).
86. Sing, K.S.W. et al. *Pure Appl. Chem.* 57 (4), 603-619 (1985).

87. Sundblom, A., Palmqvist, A.E.C., & Holmberg, K. *Langmuir* 26 (3), 1983-1990 (2010).
88. Engelhardt, G., Michel, D., III Si NMR of silicate solutions in *High-Resolution Solid-State NMR of Silicates and Zeolites* (John Wiley & Sons, 1987).
89. Nalwa, H.S. *Nanoclusters and nanocrystals, American Scientific Publishers, Stevensons Ranch* (2003).
90. Klabunde, K.J. *Nanoscale materials in chemistry, Wiley* (2001).
91. Hald, P. et al. *J. Solid State Chem.* 179 (8), 2674-2680 (2006).
92. Andersson, M., Kiselev, A., Österlund, L., & Palmqvist, A.E.C. *J. Phys. Chem. C* 111 (18), 6789-6797 (2007).
93. Holmqvist, P., Alexandridis, P., & Lindman, B. *J. Phys. Chem. B* 102, 1149-1158 (1998).
94. Nilsson, E., Furusho, H., Terasaki, O., Palmqvist A.E.C. *J. Mater. Res.* 26 (Focus Issue - Self-Assembly and Directed Assembly of Advanced Materials), 1-8 (2011).

ACKNOWLEDGEMENTS

The National Graduate School in Material Science and the Foundation for Strategic Research are acknowledged for financial support

I would also like to thank the following people:

My supervisor professor **Anders Palmqvist** for all support and advice through these years and for the ability to motivate when lack of "good" results are draining the inspiration.

Professor **Krister Holmberg** who introduced me to the subject of surface chemistry and its related research areas and for being an important source of knowledge.

Patrik Jarvol and **Åsa Östlund** for all the support and knowledge concerning the ^{29}Si-NMR measurements. I couldn't done it without you.

Yasuhrio Sakamoto for great collaborations and help in producing excellent TEM-results. Thank you for a really nice staying at Osaka Prefecture University.

Hirotoshi Furusho and **Osamu Terasaki** for valuable electron microscopy contributions to paper II and III.

Kazuteru Nonomura and **Anders Hagfeldt** for your interest in performing DSSC-measurements on my mesoporous TiO_2 materials.

My NFSM-buddies **Jonas Nordström** and **Moheb Nayeri** for collaborations and work-related discussions that has meant a lot for me.

Andreas Sundblom for supervision during my master thesis work, important silica-discussions, and for helping me with lab-work when time was running out.

My roommate **Markus Andersson** for an excellent mixture of, scientific discussions, jokes, laughs, "heavy metal" and "house". It has been a really enjoyable atmosphere.

Neo Björn Esbjörnsson for introducing me to the field of photovoltaics and for promising collaborations that hopefully will lead to more publications.

Martin Andersson, Maria Claesson, Hanna Gustafsson and **Wenxiao He** for dedicating expensive beam time at MAX-lab for my samples.

All people at Applied Surface Chemistry for shared coffee breaks and a stimulating scientific atmosphere.

My **Mother** and **Father** for all support in the early school years. I wrote the thesis but you laid the foundation.

Last but certainly not least my wife **Jenny** and my son **Simon** for always being there for me. I love you!